Journal of Sound and Vibration 546 (2023) 117450

Contents lists available at ScienceDirect

Journal of Sound and Vibration

journal homepage: www.elsevier.com/locate/jsvi

Low-frequency amplification of propeller tonal noise due to the scattering by a compact rigid cylinder

Elina Cros [a,b,*], Michel Roger [a], Gilles Serre [b]

[a] Univ Lyon, Ecole Centrale de Lyon, CNRS, Univ Claude Bernard Lyon 1, INSA Lyon, LMFA, UMR5509, 69130, Écully, France
[b] Naval Group Research, 199 avenue Pierre Gilles de Gennes, 83190 Ollioules, France

ARTICLE INFO

Keywords:
Marine propeller noise
Spinning modes
Analytical modeling
Diffraction

ABSTRACT

The present work addresses the scattering of the tonal noise of a low-speed propeller by a rigid cylinder, as a generic configuration representative of installed marine propellers. Both propeller and cylinder axes are parallel to each other. The diameters of the propeller and of the cylinder are much smaller than the acoustic wavelengths, as well as the propeller-cylinder distance. This corresponds to a compact regime of diffraction. Only the hydrodynamic tonal noise of the propeller at the first multiples of the blade-passing frequency is considered, assuming rigid blades, in a two-dimensional formulation. The direct and scattered sound fields are expressed in terms of spinning modes, with respect to the propeller and cylinder axes, respectively. Use is made of the exact Green's function of the cylinder for the Helmholtz equation. The modes of orders ± 1 are found the only efficient ones in the direct field, whereas higher-order modes rapidly decay. Yet, in the presence of the cylinder, higher-order modes are scattered into the contra-rotating mode of order 1 in the reference frame of the cylinder, with a strong amplification. A simple experiment, performed in air but with Helmholtz numbers typical of marine applications, confirms these results as key features of the asymptotic Green's function of the cylinder. The same modal behavior is reproduced as closed-form simple expressions from a low-frequency approximation of the Green's function. The results show that the installation effect is crucial for the tonal noise of marine propellers at very low frequencies.

1. Introduction

Sound generation and propagation from ships in water is a matter of concern for both the acoustic discretion of ships and the protection of aquatic wild life. It involves complex physical aspects, especially dealing with propeller-associated sound-generating mechanisms. Firstly, structure-borne noise is emitted because mechanical vibrations are transmitted to the hull through the driving shaft. Secondly, the propellers are known to generate hydrodynamic noise. The latter is generally a very significant contribution to the total noise. This is why the design of modern marine propellers has to combine better hydrodynamic efficiency and reduced emitted sound. For this, the involved mechanisms must be identified and dedicated prediction models that could be introduced at the early stages of optimization processes are needed. The most crucial aspects of marine propeller noise are the so-called installation effects, which are twofold. Firstly, the propellers are always mounted in the rear part of the ship hull, therefore they are partly embedded in a non-homogeneous and turbulent wake and/or interact with the turbulent boundary layer developing along the whole length of the hull. Random and periodic fluctuations are induced on the blades, leading to increased, respectively broadband and tonal, acoustic signatures, when compared to what the isolated propeller would radiate. This is referred to as the hydrodynamic

* Corresponding author at: Univ Lyon, Ecole Centrale de Lyon, CNRS, Univ Claude Bernard Lyon 1, INSA Lyon, LMFA, UMR5509, 69130, Écully, France.
E-mail address: elina.cros@ec-lyon.fr (E. Cros).

https://doi.org/10.1016/j.jsv.2022.117450
Received 1 March 2022; Received in revised form 13 October 2022; Accepted 16 November 2022
Available online 23 November 2022
0022-460X/

Nomenclature

Italic symbols

a	Cylinder radius
A_n	Modal amplitude in array processing
B	Blade number
c_0	Sound speed
D	Distance from cylinder axis to propeller axis
$\mathrm{e}_X, \mathrm{e}_Y, \mathrm{e}_Z$	Unit vectors of main directions
$\mathbf{F}$	Point-dipole force
$\mathbf{F}_s$	Point-dipole force harmonic
$F_s^{A,T,R}$	Fourier coefficients of axial, tangential and radial forces
G	Green's function for the Helmholtz equation
G_0	Free-field Green's function
$\mathrm{G}_{0\mathrm{as}}$	Asymptotic free-field Green's function
G_1	2-D cylinder Green's function
$\mathrm{G}_{1\mathrm{as}}$	Asymptotic cylinder Green's function
L	Distance from cylinder edge to propeller axis
$\mathrm{J}_m, \mathrm{H}_m^{(1)}$	Bessel and Hankel functions of the first kind
k	Acoustic wavenumber
m	Summation index, mode order in array processing
M	Tangential Mach number
M_n	Phase tangential Mach number
n	Spinning mode order (number of lobes)
p_{0as}, p_{1as}	Free-field and scattered pressures in asymptotic regime
$p_{\mu B}$	Complex acoustic pressure at a BPF harmonic
p_{ar}	Free-field pressure expanded as spinning modes
p_m	Sound-pressure modal amplitude
r_ϕ	Observer distance to a source-mode point
r, R_0	Circle radius
R	Observer distance to origin
s	Blade loading harmonic order
$\mathbf{x} = (r_x, \theta_x)$	Observer position
$\mathbf{y} = (r_y, \theta_y)$	Source position
(x_1, x_2)	Components of $\mathbf{x}$ in Cartesian coordinate system
(y_1, y_2)	Components of $\mathbf{y}$ in Cartesian coordinate system

Greek symbols

λ	Wavelength
μ	BPF harmonic order
Θ	Observer angle from axis
ζ	Rotor-blade force-inclination angle
ω	Angular frequency
Ω	Rotational speed
ξ	Observer angle in polar coordinates
Φ	Polar observer angle
ϕ	Polar angle of source-mode point

installation effect. In particular, stationary azimuthal distortions, defined as deviations from pure axisymmetry of the mean flow around the propeller axis, generate additional tonal noise.

Secondly, the mounting of propellers in close vicinity of the hull makes the sound radiated from the blades scattered, in such a way that the basic radiating properties of the sources are strongly modified. This is especially pronounced for the sources of the tonal noise, structured by interfering isolated-blade contributions: the vicinity of the hull introduces imbalance in the interference.

Abbreviations

BLH	Blade loading harmonic
BPF	Blade passing frequency
PSD	Power spectral densities
SPL	Sound pressure level

As a result, the noise of an installed propeller can dramatically differ from what the free-field noise would be, even considering the same sources. This second effect, addressed in the present work, is called the acoustic installation effect.

Both installation effects are usually investigated independently. The noise that would be radiated by a propeller in free field but with the real flow distortions, thus the true sources, can be predicted relying on Ffowcs Williams & Hawking's formulation of the acoustic analogy [1–3], initially developed for aeronautical applications. Indeed, the same formal background holds for air and water, basic differences being in the characteristic Mach and Reynolds numbers. The only specific features of marine propellers are the cavitation, known as a dominant source of noise in many configurations, and the more crucial role of mechanical vibrations, because of the added-mass effect of water. But cavitation noise and vibrations are discarded from the present analysis. In the analogy, the rotating blades and their accompanying unsteady flows are formally replaced by equivalent sources that are assumed to radiate in a uniform and stagnant unbounded medium. The associated wave equation is therefore usually solved with the standard free-field Green's function. Dimensional analysis indicates that, within this framework and at very low Mach numbers, the major source of noise is the passage of the propeller blades through the distortions, which generates fluctuating forces on the blades acting as equivalent acoustic dipoles [3]. This defines the so-called unsteady loading noise. The averaged force on the blades, which would be the only remaining hydrodynamic force in absence of distortion, is responsible for the steady-loading noise. Rotating blades also generate thickness noise. The latter can be modeled again from equivalent dipoles, according to Isom's formulation (see for instance Farassat [4]). Therefore, rotating dipoles are considered here as the only required generic background for the description of marine propeller noise. As long as the tonal noise at harmonics of the Blade-Passing Frequency (BPF) is considered, each tone is a sum of elementary patterns called spinning radiation modes. This notion is reminded in the paper. A mode is a diverging pressure wave, combined with an azimuthally periodic pattern spinning at some phase speed, and forced by the dipole source strength.

In the presence of surrounding surfaces, a tailored Green's function must be used or the wave equation of the analogy solved numerically with additional boundary conditions imposed on the surfaces, depending on the geometry of the latter. This has been the basis of hybrid methods developed in hydroacoustics to estimate the noise nearby the hull of a ship [5,6]. In the present work, diffraction is addressed assuming a rigid cylinder instead of a true hull geometry (Fig. 1), in order to highlight key mechanisms with a simple mathematical background. The exact tailored Green's function of the cylinder for the Helmholtz equation is used to this end, the problem being stated in the frequency domain. Indeed, diffraction is a matter of compared source-to-obstacle distance and acoustic wavelength. The consequence is that the amount of scattering differs for all angular positions of a blade element seen as source along its circular path. This causes imbalance in the partial cancellations which determine the radiation efficiency of a spinning mode. In order to take this exactly into account in the study, each spinning mode is reproduced with an equivalent circular distribution of stationary phased dipoles, referred to as a source-mode [7,8].

Installed marine propellers correspond to very compact configurations, in the sense that both the blade-tip radius and the distance to the ship hull are much smaller than the emitted acoustic wavelengths. This is especially true in the very-low frequency range corresponding to the first harmonics of the BPF (Blade-Passing Frequency, defined as the rotational frequency $\Omega/(2\pi)$ multiplied by the number of blades B), investigated in the present work. Typically, for a BPF of 30 Hz and a sound speed of 1500 m/s, the Helmholtz number built of some characteristic length Λ remains below 0.1 for values of Λ up to 8 m. This confirms that the propeller–hull distance, and to some extent also the region including the blades and the hull cross-section, is acoustically compact. Therefore, the source-modes must be assumed in the very vicinity of the cylinder to be representative of a marine application. A compact approximation of the Green's function is justified in such cases, in the sense introduced by Howe [9]. This particular regime is crucial because it is known to produce a more or less pronounced amplification of the sound from sources of high equivalent polar orders. The amplification has been reported in similar studies, based on asymptotic analyses performed on exact Green's functions [10,11], for sources approaching the edge of a rigid half-plane.

The aforementioned context motivated the authors in addressing specifically the compact regime of the scattering of a source-mode by a rigid cylinder. The configuration is understood as a generic one, representative of a marine propeller installed close to a ship hull. It is mainly addressed here with a two-dimensional model, in order to provide a first insight into the underlying physics with minimum mathematical complexity. Three-dimensional aspects are also discussed shortly; they confirm the basic addressed mechanisms, already highlighted with the two-dimensional analysis, only adding secondary refinements. In fact, the main scattering features involve the directions normal to the cylinder surface, giving less importance to the contribution from axial blade forces. In that sense, the three-dimensional problem statement is not essential. A dedicated experiment has also been carried out in air, in an anechoic room, in order to validate the relevance of the two-dimensional model. The setup includes a small-size three-bladed propeller operated close to a rigid cylinder, with ratios of wavelengths to dimensions representative of marine applications. The study is aimed at pointing out that the diffraction is able to generate much higher sound than the direct source-mode radiation in free field.

Approximations, only relevant for the presently addressed aspects of marine propellers, are considered in this work. The effects of fluid motion are neglected, when formulating sound propagation and scattering problems, assuming a uniform propagation medium at rest. Local azimuthal flow distortions are indirectly accounted for by the associated induced blade forces, acting as sources. More advanced formulations would be needed for aeronautical applications, corresponding to non-compact configurations and much higher Mach numbers. In particular, the refraction of sound by mean-flow gradients would need to be considered (see, for instance, the integral formulation proposed by Mancini et al. [?], for weakly non-uniform flows). Efficient formulations have also been developed for surfaces in a moving fluid, such as the time-domain formulation described by Wang et al. [?]. Such approaches are far beyond what the present work is aimed at. In the marine-propeller context, the characteristic Mach numbers are vanishing and the lengths scales of the mean-flow gradients are much smaller than the acoustic wavelengths. Refraction and sound convection by flow are negligible phenomena, compared to the addressed sound scattering.

Some theoretical background of tonal rotating-blade noise for compact blades and the notion of associated source-modes are reminded in Section 2. The analytical expressions of the scattered sound field based on the two-dimensional tailored Green's function of the rigid cylinder for the Helmholtz equation are derived in Section 3. The developments specific to the asymptotic regime for a far-field observer and arbitrary source-modes are detailed in Section 4. The aim is to highlight the amplification caused by cylinder scattering at very low frequencies. The effects of the source-to-cylinder distance and of other key parameters are discussed. The accompanying experiment is described in Section 5, where the main results are discussed, confirming the amplification mechanism. The effect of the hub of a propeller is shortly addressed in Section 6, as a complementary topic. Finally, three-dimensional considerations are given in Section 7.

2. Free-field tonal noise formulation

Before addressing the theoretical model of sound scattering by a rigid cylinder, elementary expressions for the acoustic pressure radiated by a propeller in the far field are reviewed in this section. The fluid motion relative to the reference frame of the propeller is neglected when describing sound propagation, in view of the negligibly small Mach numbers. In a second step, the rotating blades are replaced by equivalent stationary sources. The far-field expressions are considered only as a reference for the analysis of the modal properties of the radiated field.

2.1. Rotating-blade noise formulation

Tonal rotor noise is usually formulated in the frequency domain in the far-field, relying on Ffowcs Williams & Hawkings' formulation of the acoustic analogy [1,2]. The mathematical solution is reminded in this section as a background for the present developments, assuming a single, acoustically compact, blade element rotating at constant angular speed Ω on the circle of radius r in a quiescent propagation medium. Details can also be found in Refs. [12,13]. With the conventional notation $\mathrm{e}^{-\mathrm{i}\omega t}$ for monochromatic waves of angular frequency ω, the complex-valued amplitude of the far-field acoustic pressure at the multiple of order μ of the BPF, $\omega = \mu B \Omega$ reads

$$p_{\mu B}(\mathbf{x}) = \frac{\mathrm{i}\, k_{\mu B} B}{4\pi R}\, \mathrm{e}^{\mathrm{i}\, k_{\mu B} R} \sum_{s=-\infty}^{\infty} \mathrm{e}^{\mathrm{i}\,(\mu B - s)(\Phi - \pi/2)} \tag{1}$$
$$\times \left\{ \mathrm{J}_{\mu B - s}\,(\mu B\, M\, \sin\Theta) \left[F_s^A \cos\Theta - \frac{(\mu B - s)\, F_s^T}{\mu B\, M} \right] + \mathrm{i}\, \sin\Theta\, F_s^R\, \mathrm{J}'_{\mu B - s}\,(\mu B\, M\, \sin\Theta) \right\},$$

with the notations defined in Fig. 1, where $M = \Omega r / c_0$ is the tangential Mach number of the element and $k_{\mu B} = \mu B \Omega / c_0$ is the acoustic wavenumber. The observer is defined by the spherical coordinates (R, Θ, Φ) in the reference frame $(\mathbf{e}_X, \mathbf{e}_Y, \mathbf{e}_Z)$. In the general case, Eq. (1) is summed over all elements of a discretized blade. For very compact blades, all dimensions of which remain much smaller than the acoustic wavelengths, a single element carrying the instantaneous integrated force is used, located at some averaged radius $r = R_0$. This simplification, relevant for free-field assessment, can no longer be accepted for diffraction studies, because sources of different radius are scattered differently, as confirmed later on in this work.

The complex-valued factors $F_s^{A,T,R}$ are the Fourier coefficients of the axial, tangential and radial components of the hydrodynamic force $\mathbf{F}(t)$ on the element, acting as a point dipole. The total Fourier coefficients F_s are related to the algebraic value of the force $F(t)$ by the definition

$$F(t) = \sum_{s=-\infty}^{\infty} F_s\, \mathrm{e}^{-\mathrm{i}\, s\, \Omega t}, \qquad F_s = \frac{\Omega}{2\pi} \int_0^{2\pi/\Omega} F(t)\, \mathrm{e}^{\mathrm{i}\, s\, \Omega t}\, \mathrm{d}t\,. \tag{2}$$

In the plane of the rotor disk considered later on for two-dimensional diffraction studies, $\Theta = \pi/2$ and the formula reduces to

$$p_{\mu B}(\mathbf{x}) = \frac{\mathrm{i}\, k_{\mu B} B}{4\pi R}\, \mathrm{e}^{\mathrm{i}\, k_{\mu B} R} \sum_{s=-\infty}^{\infty} \mathrm{e}^{\mathrm{i}\, n(\Phi - \pi/2)} \left\{ -n\, F_s^T \frac{\mathrm{J}_n(\mu B\, M)}{\mu B\, M} + \mathrm{i}\, F_s^R\, \mathrm{J}'_n(\mu B\, M) \right\}, \tag{3}$$

introducing $n = \mu B - s$. Eq. (1) states that a tone involves a linear combination of radiation modes. Keeping in mind the time dependence $\mathrm{e}^{-\mathrm{i}\,\omega t}$, a single mode at the frequency $\omega = \mu B\, \Omega$ is defined as a pressure pattern with n angular periods called lobes, the phase of which spins at the angular velocity $\mu B\, \Omega / n$ associated with a tangential phase Mach number $M_n = \mu B\, \Omega\, r / (n\, c_0)$, if r stands for the radius at which the sources of the mode are considered. The angular dependency would be the same in a two-dimensional

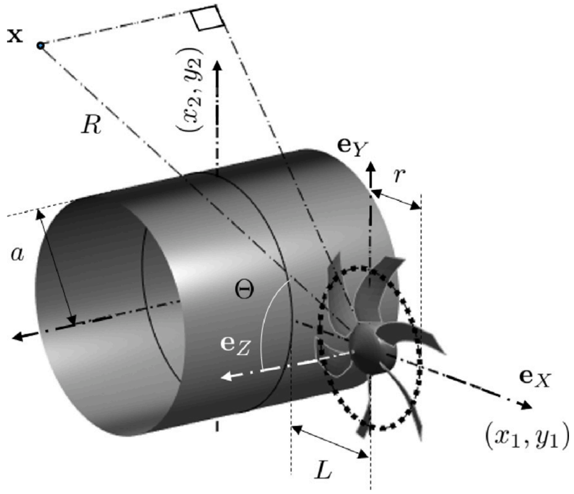

Fig. 1. Propeller and cylinder reference frames, with spherical coordinates for the three-dimensional formulation of propeller noise. Discretized source-mode of radius r featured by the circular array of dots. Subsequent developments refer to the rotor-disk plane $(\mathbf{e}_X, \mathbf{e}_Y)$.

description, but the spherical spreading with which it combines would be replaced by cylindrical spreading. In the plane $\Theta = \pi/2$, the symmetric mode associated with the Bessel function J_0 and with the BLH of order $s = \mu B$ can only be excited by the radial force component. The truncation of the infinite sum in Eq. (1) needed for practical predictions is determined by the properties of the Bessel functions: for a fixed value of the argument, the functions rapidly go to zero for absolute orders exceeding the argument. The blades of a propeller operating in an arbitrary stationary distortion experience a range of BLH orders s. Only a limited interval of them, say between $\mu B - n_{max}$ and $\mu B + n_{max}$ where n_{max} is some integer, possibly give rise to efficient radiation at the frequency $\omega = \mu B\,\Omega$, because of the weighting by the Bessel function. The range is wider or narrower, depending on either the distortion is concentrated or spread.

For marine propellers, the tangential Mach number $\Omega r/c_0$ is very small, typically about 0.02 at 30 m/s, so that for moderate blade numbers and BPF harmonic orders, the argument of the Bessel functions is also small. Furthermore, the tangential phase Mach number M_n is always smaller than 1 for any order $n \neq 0$ (the definition makes no sense for the symmetric mode $n = 0$). Even in non-compact cases, the condition $M_n \ll 1$ corresponds to a negligible radiation efficiency. This makes very poor sound expected in free field from the modal structure of marine propellers, except if the symmetric mode is excited, with $s = \mu B$, for the axial component of blade forces. Therefore, Taylor expansions can be performed to provide a relevant approximation. The limit forms of Bessel functions for small arguments read [14]

$$\mathrm{J}_{|n|}(\mu B\,M) \sim \left(\frac{\mu B\,M}{2}\right)^{|n|}, \qquad \mathrm{J}_0(\mu B\,M) \sim 1,$$

$$\mathrm{J}'_{|n|}(\mu B\,M) \sim \frac{1}{2}\left(\frac{\mu B\,M}{2}\right)^{|n|}, \qquad \mathrm{J}'_0(\mu B\,M) \sim -\frac{\mu B\,M}{2}.$$

The ratio

$$\frac{\mathrm{J}_{|n|}(\mu B\,M)}{\mu B\,M} \sim \frac{1}{2^{|n|}}\,(\mu B\,M)^{|n|-1}$$

becomes negligible for $|n| \geq 2$, whereas it is $1/2$ for $|n| = \pm 1$. This makes the mode orders ± 1 the only significantly contributing ones. These special aspects of vanishing Mach numbers will be re-addressed in Section 4.3. Though typical of marine propellers, they are also believed to hold, to a minor extent, for some small-size, very low-speed fans used in air, and for some small-size drone propellers. In that sense, the present work has possible applications in both hydroacoustics and aeroacoustics.

2.2. Source-mode expansion

The sound field of a single mode of order n in Eq. (1) can be exactly reproduced by continuously distributing phased stationary sources of equal amplitude over the circle of radius r, provided that the phase is tuned to simulate the angular velocity $\mu B\,\Omega/n$. The amplitude is defined by the BLH F_s. Therefore, the phase at any angle ϕ on the circle is defined by the factor $\mathrm{e}^{\mathrm{i}\,n\phi}$. Such a distribution is called a source-mode in the present work. Its main interest is that it provides a representation of the sound field valid at every point in space and not only in the far field, as discussed in Refs. [7,11,15]. In particular, this allows to take into account the near-field terms involved in the scattering by neighboring surfaces. The stationary point dipole of a source-mode at the angle ϕ in Fig. 2 has the same instantaneous strength $F(\phi, t)$ as the dipole at angle $\phi = 0$ but with a time delay $\Delta t = (\mu B - s)\,\phi/\omega$:

$$\forall \phi \in [0, 2\pi], \quad F(\phi, t) = F\left(0, t - (\mu B - s)\phi/\omega\right). \tag{4}$$

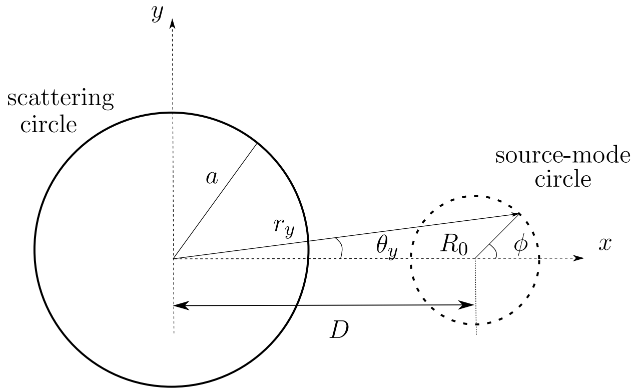

Fig. 2. Coordinates of a source mode close to a scattering cylinder for the asymptotic calculations. Note that $D = L + a$ (see Fig. 1).

This forces the wanted spinning pattern of angular phase speed Ω_s with $n = \mu B - s$. For the mode of order n associated with the blade-loading harmonic of order s, $F(\phi, t) = F_s\, \mathrm{e}^{-\mathrm{i}\,\mu B\,\Omega t}$ with $F_s = A\, \mathrm{e}^{\mathrm{i}\, n\phi}$, A being a constant.

3. Cylinder scattering

3.1. Two-dimensional cylinder Green's function

An alternative to numerical implementations of the Green's formula, when solving a problem of acoustics in the presence of solid boundaries, is to consider a Green's function tailored to the geometry. In the present generic configuration, the sources are assumed close to a rigid cylinder of circular cross-section. The exact Green's function, $\mathrm{G}(\mathbf{x}, \mathbf{y})$, solution of the homogeneous Helmholtz equation, is determined by adding to the free-field Green's function G_0 a secondary Green's function G_1 accounting for the scattered field. This scattered part G_1 corresponds to equivalent sources distributed on the surface. Therefore, it is expressed in terms of cylindrical harmonics. The term G_0 must also be expanded on the same set of harmonics, in order to formulate the rigid-wall boundary condition on the cylinder surface, that must be fulfilled by the complete Green's function $\mathrm{G} = \mathrm{G}_0 + \mathrm{G}_1$. The procedure is detailed, for instance, in [16]. In polar coordinates with origin at the center of the cylinder cross-section, and for an observer radius larger than the source radius ($r_x \geq r_y$), the tailored Green's function reads

$$
\begin{aligned}
\mathrm{G}(\mathbf{x}, \mathbf{y}) = {} & \frac{-\mathrm{i}}{4} \left[\mathrm{J}_0\left(k r_y\right) - \frac{\mathrm{J}_0'(ka)}{\mathrm{H}_0^{(1)\prime}(ka)} \mathrm{H}_0^{(1)}\left(k r_y\right) \right] \mathrm{H}_0^{(1)}\left(k r_x\right) \\
& - \frac{\mathrm{i}}{4} \sum_{m=1}^{\infty} 2\cos[m(\theta_y - \theta_x)] \left[\mathrm{J}_m\left(k r_y\right) - \frac{\mathrm{J}_m'(ka)}{\mathrm{H}_m^{(1)\prime}(ka)} \mathrm{H}_m^{(1)}\left(k r_y\right) \right] \mathrm{H}_m^{(1)}\left(k r_x\right)
\end{aligned} \tag{5}
$$

if a stands for the cylinder radius. x and y as indices stand for the observer and source coordinates, respectively. In the opposite configuration ($r_x < r_y$), the products $\mathrm{J}_m\left(k r_y\right) \mathrm{H}_m^{(1)}\left(k r_x\right)$ corresponding to the first terms in the squared brackets must be replaced by $\mathrm{H}_m^{(1)}\left(k r_y\right) \mathrm{J}_m\left(k r_x\right)$. In fact, these terms stand for the free-field Green's function $\mathrm{G}_0(\mathbf{x}, \mathbf{y})$, expressed in the coordinate system of the cylinder. The other terms involving ratios of derivatives account for the scattering by the cylinder. All exact calculations performed in the present work, for arbitrary dipole source-modes, are performed by making the scalar product of the local dipole strength by the first gradient of the Green's function G with respect to the source coordinates. This provides the value of the radiated sound field at any point of space as

$$
p = \mathbf{F}_s \cdot \boldsymbol{\nabla}(\mathrm{G}_0 + \mathrm{G}_1),
$$

with $\mathbf{F}_s = F_s\, \mathbf{n}_\phi$, where $\mathbf{n}_\phi$ is the unit vector along the dipole axis of angular location ϕ along the source-mode circle and $F_s = F\, \mathrm{e}^{\mathrm{i}\, n\phi}$ is the dipole strength. The derivations of $\nabla(\mathrm{G}_0 + \mathrm{G}_1)$ are not detailed here for conciseness. They are similar to those provided by Gloerfelt et al. [17], who investigated the radiation of quadrupoles in the presence of a cylinder. The scattering is calculated for each point dipole of a source-mode and the total field is obtained through an integral over the circle. Practically, this integral is discretized as a finite sum for implementation. A similar approach has been detailed by Roger & Moreau [11] in the investigation of the scattering of fan/propeller noise in the air by the edge of a rigid half-plane.

3.2. Greens' function formulation in the asymptotic regime

The asymptotic analysis leading to the compact regime of the Green's function is mainly focused on the part G_1, responsible for amplification. However, special cases also require a comparison with the direct field. Let us note:

$$\frac{\mathrm{J}_0'(ka)}{\mathrm{H}_0^{(1)\prime}(ka)} = \frac{\mathrm{J}_1(ka)}{\mathrm{H}_1^{(1)}(ka)} = \Phi_0\,, \qquad \frac{\mathrm{J}_m'(ka)}{\mathrm{H}_m^{(1)\prime}(ka)} = \frac{\mathrm{J}_{m-1}(ka)-\mathrm{J}_{m+1}(ka)}{\mathrm{H}_{m-1}^{(1)}(ka)-\mathrm{H}_{m+1}^{(1)}(ka)} = \Phi_m.$$

Consider an observer in the acoustic far field and distributed sources over a circle remaining close to the scattering cylinder, the latter being acoustically compact, so that

$$kr_x \gg 1\,, kr_y \ll 1\,, ka \ll 1\,,$$

In the present application, source points are distributed over a circle of radius R_0, the center of which is at some small distance D from the center of the cylinder, in such a way that also $kD \ll 1$ and $kR_0 \ll 1$ (circular arrays of dots in Figs. 1 and 2). This refers to the so-called compact Green's function framework. In this case, asymptotic expansions can be used to derive a simplified form of the Green's function. For large arguments [14],

$$\mathrm{H}_m^{(1)}\left(kr_x\right) \sim \sqrt{\frac{2}{\pi\, kr_x}}\,\mathrm{e}^{\mathrm{i}\,[kr_x - m\pi/2-\pi/4]},$$

whereas for small arguments

$$\mathrm{H}_m^{(1)}\left(kr_y\right) \sim \frac{-\mathrm{i}}{\pi}\,\Gamma(m)\left(\frac{2}{kr_y}\right)^m \quad \text{and} \quad \mathrm{J}_m\left(kr_y\right) \sim \frac{1}{\Gamma(m+1)}\left(\frac{kr_y}{2}\right)^m, m \ge 1$$

$$\mathrm{H}_0^{(1)}\left(kr_y\right) \sim \frac{2\mathrm{i}}{\pi}\ln\left(\frac{kr_y}{2}\right) \quad \text{and} \quad \mathrm{J}_0\left(kr_y\right) \sim 1-\left(\frac{kr_y}{2}\right)^2.$$

Introducing these developments in the definition of the factor Φ_m for small values of ka yields

$$\Phi_0 \sim \mathrm{i}\pi\left(\frac{ka}{2}\right)^2, \qquad \Phi_m \sim \frac{-\mathrm{i}\pi}{\Gamma(m)\,\Gamma(m+1)}\left(\frac{ka}{2}\right)^{2m}.$$

For consistency, ka and kr_y must be assumed as small quantities of the same order of magnitude.

Once introducing the asymptotic developments in the expression of the exact Green's function, the first step to the limit form of the Green's function G_1 is obtained as

$$\mathrm{G}_{1as}(\mathbf{x},\mathbf{y}) \sim \frac{-\mathrm{i}}{4}\,f(r_x)\left(\frac{ka}{2}\right)^2 2\ln\left(\frac{kr_y}{2}\right) - \frac{\mathrm{i}}{4}\,f(r_x)\sum_{m=1}^{\infty} 2\cos[m(\theta_y-\theta_x)]\,\frac{\mathrm{e}^{-\mathrm{i}\,m\pi/2}}{\Gamma(m+1)}\left(\frac{ka}{2}\right)^m\left(\frac{a}{r_y}\right)^m \tag{6}$$

with

$$f(r_x) = \sqrt{\frac{2}{\pi\, kr_x}}\,\mathrm{e}^{\mathrm{i}\,[kr_x-\pi/4]}.$$

Next assuming that a/r_y is of order 1 leads to retain only the leading term $m = 1$. Finally

$$\mathrm{G}_{1as}(\mathbf{x},\mathbf{y}) \sim \frac{-\mathrm{i}}{2}\,f(r_x)\left(\frac{ka}{2}\right)^2\left[\ln\left(\frac{kr_y}{2}\right) - \mathrm{i}\,\cos(\theta_y-\theta_x)\left(\frac{2}{kr_y}\right)\right]. \tag{7}$$

Space derivatives of the Green's function with respect to source coordinates are required when calculating the sound from dipoles. In the radial derivative the logarithm can be neglected as negligible compared to the other term. The first gradient components are finally obtained as

$$\frac{\partial \mathrm{G}_{1as}}{\partial r_y} = f(r_x)\left(\frac{ka}{2}\right)^2\frac{\cos(\theta_y-\theta_x)}{kr_y^2}, \qquad \frac{1}{r_y}\frac{\partial \mathrm{G}_{1as}}{\partial \theta_y} = f(r_x)\left(\frac{ka}{2}\right)^2\frac{\sin(\theta_y-\theta_x)}{kr_y^2}. \tag{8}$$

It is worth noting that the compact Green's function and its derivatives no longer involve indices $m > 1$.

3.3. Asymptotic free-field Green's function

Subsequent needs also require the derivatives of the free-field Green's function G_0. In the compact regime, the latter reads

$$\mathrm{G}_{0as}(\mathbf{x},\mathbf{y}) \sim \frac{-\mathrm{i}}{4}\,f(r_x)\left[1-\left(\frac{kr_y}{2}\right)^2 - 2\,\mathrm{i}\,\cos[(\theta_y-\theta_x)]\left(\frac{kr_y}{2}\right)\right]. \tag{9}$$

For the radial derivative, the term $\left(kr_y/2\right)^2$ can be discarded as negligible compared to the other terms. Finally, the approximations are obtained as:

$$\frac{\partial \mathrm{G}_{0as}}{\partial r_y} = -\frac{k}{4}\,f(r_x)\cos(\theta_y-\theta_x)\,, \qquad \frac{1}{r_y}\frac{\partial \mathrm{G}_{0as}}{\partial \theta_y} = \frac{k}{4}\,f(r_x)\sin(\theta_y-\theta_x)\,, \tag{10}$$

with

$$f(r_x) = \sqrt{\frac{2}{\pi\, kr_x}}\, \mathrm{e}^{\mathrm{i}\,[kr_x - \pi/4]}.$$

4. Radiation of compact spinning source-modes

The expressions of the previous section are now used to calculate the far-field sound pressure radiated by a compact source mode of arbitrary order. Derivations are first detailed for purely tangential dipoles; the case of radial dipoles is then summarized for completeness.

4.1. Point-dipole formula

In the present section, for any point dipole of a source mode, the dipole axis is assumed tangent to the source-mode circle. This restriction would be exact for a purely axial-flow propeller, with unswept blades. With the notations in Fig. 2, the point dipole of angular coordinate ϕ along the source circle and of unit strength has the radial and angular components in the reference frame of the scattering cylinder

$$F_r = -\frac{D}{r_y}\, \sin\phi\, \mathrm{e}^{\mathrm{i}\,n\phi}\,, \qquad F_\theta = \frac{R_0 + D\, \cos\phi}{r_y}\, \mathrm{e}^{\mathrm{i}\,n\phi}\,,$$

for the spinning mode of order n, with

$$r_y^2 = D^2 + R_0^2 + 2\, D R_0\, \cos\phi\,, \qquad \tan\theta_y = \frac{\sin\phi}{\cos\phi + D/R_0}.$$

The scattered sound pressure of the point dipole in the asymptotic regime reads

$$p_{1as}(r_x, \theta_x) = F_r\, \frac{\partial \mathrm{G}_{1as}}{\partial r_y} + \frac{F_\theta}{r_y}\, \frac{\partial \mathrm{G}_{1as}}{\partial \theta_y},$$

After rearranging terms:

$$\frac{k\, p_{1as}(r_x, \theta_x)}{f(r_x)\,(ka/2)^2} = \cos\theta_x\, (R_0^2 - D^2)\, \frac{\sin\phi\, \mathrm{e}^{\mathrm{i}\,n\phi}}{r_y^4} - \sin\theta_x\, \left[(R_0^2 + D^2)\, \frac{\cos\phi\, \mathrm{e}^{\mathrm{i}\,n\phi}}{r_y^4} + 2\, R_0 D\, \frac{\mathrm{e}^{\mathrm{i}\,n\phi}}{r_y^4} \right] \tag{11}$$

According to the same principles as for the diffracted field, the direct sound pressure radiated by the point dipole in the asymptotic regime is :

$$p_{0as}(r_x, \theta_x) = F_r\, \frac{\partial \mathrm{G}_{0as}}{\partial r_y} + \frac{F_\theta}{r_y}\, \frac{\partial \mathrm{G}_{0as}}{\partial \theta_y}$$

After developing terms, it is expressed as

$$\begin{aligned} \frac{p_{0as}(r_x, \theta_x)}{f(r_x)\,(k/4)} = {} & \cos\theta_x \left[(R_0^2 + D^2)\, \frac{\sin\phi\, \mathrm{e}^{\mathrm{i}\,n\phi}}{r_y^2} + 2\, R_0 D\, \frac{\cos\phi\, \sin\phi\, \mathrm{e}^{\mathrm{i}\,n\phi}}{r_y^2} \right] \\ & - \sin\theta_x \left[(R_0^2 + D^2)\, \frac{\cos\phi\, \mathrm{e}^{\mathrm{i}\,n\phi}}{r_y^2} + R_0 D\, \frac{\mathrm{e}^{\mathrm{i}\,n\phi}}{r_y^2} + R_0 D\, \frac{\cos 2\,\phi\, \mathrm{e}^{\mathrm{i}\,n\phi}}{r_y^2} \right] \end{aligned} \tag{12}$$

The total sound of the source mode is obtained by performing the integration on the circle for Eq. (11) and Eq. (12), from $\phi = -\pi$ to $\phi = +\pi$. The resulting closed-form expressions are developed in the next section.

4.2. Case of higher-order modes

From the previous section, three integrals involving the quantities $\cos\phi$, $\sin\phi$ and $\mathrm{e}^{\mathrm{i}\,n\phi}$ and the factor r_y^4 in the denominator must be calculated. These integrals are detailed in Appendix. Regrouping all terms in the developed expression of the acoustic pressure leads to the final result

$$p_{1as}(r_x, \theta_x) \sim -\mathrm{i}\frac{\pi\, k}{4}\, n\, \left(\frac{a}{D}\right)^2 \left(\frac{-R_0}{D}\right)^{n-1}\, \mathrm{e}^{-\mathrm{i}\,\theta_x} \sqrt{\frac{2}{\pi\, kr_x}}\, \mathrm{e}^{\mathrm{i}\,(kr_x - \pi/4)}\,. \tag{13}$$

The most important feature is that, whatever the positive order n of the source mode is, the asymptotic scattering by the compact Green's function of the cylinder generates the mode $m = -1$, thus with a single lobe and spinning in the opposite direction. The factor $n\,(-R_0/D)^{n-1}$ is involved in the amplification of the direct mode. Of course, the mode $m = +1$ is similarly produced for any negative order n.

In order to assess the asymptotic formulation, the decrease of the scattered sound with observer distance r_x is plotted in Fig. 3, for a source-mode located at the dimensionless distance $kL = 0.1$ from the cylinder edge and various mode orders $n > 1$. The global compactness is ensured for all configurations. The sound pressure level is averaged over a full circle $\theta_x \in [0, 2\pi]$. The dashed and solid lines stand for the exact analytical solution, Eq. (5), and for the asymptotic formulation, Eq. (13), respectively. The

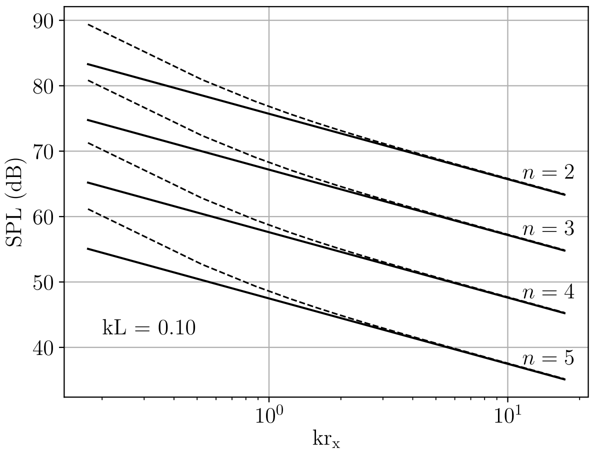

Fig. 3. Sound pressure level decrease of a source-mode located nearby a rigid cylinder for higher-order modes, $n > 1$. $kR_0 = 0.034$, $R_0/D = 0.25$, $kL = 0.10$. Exact (- - -) and asymptotic (—) solutions.

results are twofold. Firstly, both solutions nearly coincide beyond $kr_x = 3$, where the far-field decay $1/\sqrt{r_x}$ is reached. Secondly, the amplitude of the scattered pressure decreases as the mode order increases, for the same dipole source strength, as expected from the factor $n(R_0/D)^{n-1}$. More precisely, overall level differences of about 8.6 dB, 9.6 dB, 10.2 dB are predicted from the term $20\log_{10}[n(R_0/D)^{n-1}]$ between the scattered sounds of the pairs of mode orders ($n = 2, n = 3$), ($n = 3, n = 4$) and ($n = 4, n = 5$), respectively . The same test for special cases is also reported in Fig. 4 in the next section.

The amplification itself is better recognized if now the free field of the same arbitrary mode $n > 1$ is calculated, also referring to the same asymptotic developments, from Eqs. (12). The integrals involved in the formulation are developed in Appendix. Reproducing similar derivations as for the function G_{1as} with the same source mode now leads to an exactly zero pressure field. This means that, at the leading order of the asymptotic regime, the free field contribution is negligible compared to the scattered field, confirming the amplification mechanism.

4.3. Special cases

Eq. (13) of the previous section holds for $n \geq 2$. Special developments are required for the mode $n = 1$, leading to consider the new integrals in Appendix. When this is applied to derive the radiation of the source-mode $n = 1$, the expression follows as

$$p_{1as}(r_x, \theta_x) \sim -\mathrm{i}\,\frac{\pi k}{4}\left(\frac{a}{D}\right)^2 \mathrm{e}^{-\mathrm{i}\,\theta_x}\sqrt{\frac{2}{\pi\, kr_x}}\,\mathrm{e}^{\mathrm{i}(kr_x-\pi/4)}\,. \tag{14}$$

Again the mode -1 is found in the scattered field (the expression is in fact Eq. (13) with $n = 1$) but now the direct field derived following the same principles is expressed as :

$$p_{0as}(r_x, \theta_x) \sim \mathrm{i}\,\frac{\pi k}{4}\,\mathrm{e}^{\mathrm{i}\,\theta_x}\sqrt{\frac{2}{\pi\, kr_x}}\,\mathrm{e}^{\mathrm{i}(kr_x-\pi/4)}\,, \tag{15}$$

which corresponds to significant radiation, of similar efficiency as for the scattered field. The asymptotic scattering causes no amplification in this case, unlike for higher-order modes, since the factor a/D is smaller than 1. Eq. (14) is a minor perturbation of the direct field, Eq. (15). This is confirmed by the test reported in Fig. 4. The exact and asymptotic solutions of the direct and scattered parts for the special case $n = 1$, averaged over all observation angles, are plotted as a function of the observer distance. The level difference of about 5 dB between the scattered and direct sounds is well predicted by the far-field estimate $20\log_{10}(a/D)^2$ from Eqs. (14) and (15). Then, as seen previously for higher-order modes, both solutions perfectly match above $kr_x = 3$, which defines the validity limit of the asymptotic formulation.

The special behavior of the mode $n = 1$ can be explained by simple physical considerations. For this mode, two diametrically opposite dipoles are in phase opposition, which means that they point in the same direction. They double each other in amplitude because the diameter is acoustically compact. The total source mode is equivalent to a spinning point dipole.

A similar discussion can be made about the symmetric source mode $n = 0$, for which diametrically opposite dipoles now point in opposite directions because they are in phase. They cancel each other, so that the expected radiation of the mode is zero in the compact limit. This can be verified easily by repeating the previous analysis in the case $n = 0$: both the asymptotic free field and the asymptotic scattered field are zero. Important consequences follow when transposing these results to installed marine propellers. The symmetric mode is known to be only generated by interaction of the propeller with the distortion harmonic of order $s = \mu B$ at any BPF order μ. It should not be a major issue, unlike in the case of aircraft propellers, because it cannot experience amplification by hull scattering. In contrast, the analysis reveals that the modes $n = \pm 1$ are expectedly the most efficient ones, both in free field

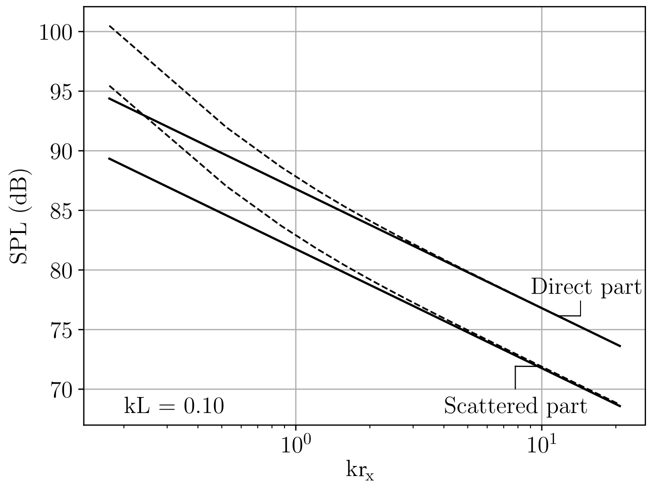

Fig. 4. Sound pressure level decrease of a source-mode located nearby a rigid cylinder for the mode $n = 1$. $kR_0 = 0.034$, $R_0/D = 0.25$, $kL = 0.10$. Exact (- - -) and compact approximations (—) of the direct and scattered parts of the Green's function.

and in the presence of a hull. These modes are likely to be excited at the lowest frequencies for installed propellers with quite small blade numbers.

It is worth noting that the selective amplification associated with asymptotic scattering leads to the possible need to reconsider the assumption of a single equivalent dipole on each blade, even if the blade is compact. Indeed, source points close to blade tip and close to hub experience different amounts of scattering. Such a 'de-compacification' is beyond the scope of the present study.

4.4. Case of a radial force

The complementary case of a radial force component in the sense of the propeller or of the modal circle is considered in this section for completeness. Indeed, such a dipole is part of the loading noise of a twisted swept blade, even if not dominant in an axial-flow architecture. Furthermore, formulations of the thickness noise detailed, for instance, in Refs. [1,3], involve a radial dipole associated with the centripetal acceleration. In the reference frame of the cylinder in Fig. 2, the radial and tangential components of a point dipole of angle ϕ become

$$F_r = \frac{R_0 + D\cos\phi}{r_y}\,\mathrm{e}^{\mathrm{i}\,n\phi}, \qquad F_\theta = \frac{D}{r_y}\,\sin\phi\,\mathrm{e}^{\mathrm{i}\,n\phi},$$

and the far-field scattered pressure is deduced as

$$\frac{k\,p_{1as}(r_x,\theta_x)}{f(r_x)\,(ka/2)^2} \simeq \sin\theta_x\,(R_0^2 - D^2)\,\frac{\sin\phi\,\mathrm{e}^{\mathrm{i}\,n\phi}}{r_y^4} + \cos\theta_x\left[(R_0^2 + D^2)\,\frac{\cos\phi\,\mathrm{e}^{\mathrm{i}\,n\phi}}{r_y^4} + 2\,R_0 D\,\frac{\mathrm{e}^{\mathrm{i}\,n\phi}}{r_y^4}\right]. \tag{16}$$

The derivations can be repeated, using the same integrals as for the tangential dipoles. They lead to the very similar result for the case of higher modes, $n \geq 2$:

$$p_{1as}(r_x,\theta_x) \sim \frac{\pi\,k}{4}\,n\left(\frac{a}{D}\right)^2\left(\frac{-R_0}{D}\right)^{n-1}\mathrm{e}^{-\mathrm{i}\,\theta_x}\sqrt{\frac{2}{\pi\,kr_x}}\,\mathrm{e}^{\mathrm{i}\,(kr_x-\pi/4)}, \tag{17}$$

$$p_{0as}(r_x,\theta_x) \sim 0, \tag{18}$$

which differs from Eq. (13) only by a phase quadrature. This difference is also found in the special case $n = 1$, where the scattered and the direct field read:

$$p_{1as}(r_x,\theta_x) \sim -\mathrm{i}\,\frac{\pi\,k}{4}\left(\frac{a}{D}\right)^2\mathrm{e}^{-\mathrm{i}\,\theta_x}\sqrt{\frac{2}{\pi\,kr_x}}\,\mathrm{e}^{\mathrm{i}\,[kr_x+\pi/2-\pi/4]}, \tag{19}$$

$$p_{0as}(r_x,\theta_x) \sim \mathrm{i}\,\frac{\pi\,k}{4}\,\mathrm{e}^{\mathrm{i}\,\theta_x}\sqrt{\frac{2}{\pi\,kr_x}}\,\mathrm{e}^{\mathrm{i}\,[kr_x+\pi/2-\pi/4]}. \tag{20}$$

For the mode $n = 1$, the result is due to the fact that diametrically opposite radial dipoles are again aligned and double each other in the compact limit. The resulting equivalent point dipole is just spinning with an angular phase shift of $\pi/2$ with respect to the point dipole of the tangential-force mode because they are perpendicular to each other.

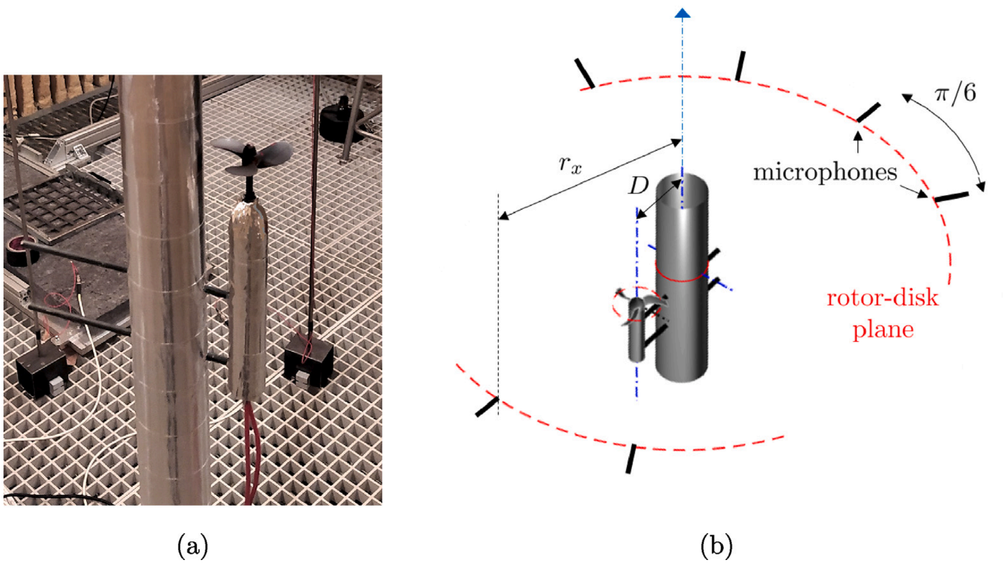

Fig. 5. (a): picture of the small-scale propeller-cylinder mockup installed in the anechoic room of Ecole Centrale de Lyon. (b): sketch of the setup for measurements in the propeller-disk plane (featured by red circles). (For interpretation of the references to color in this figure legend, the reader is referred to the web version of this article.)

The amplification inherent to the compact scattering of source-modes, described in this section, is specific to the rigid cylinder. It must be distinguished from previously reported amplification effects by bodies of other shapes. Typically, a source-mode is also amplified as its circle approaches the edge of a rigid half-plane, but the spinning-mode character is lost and replaced by a cardioid radiation pattern, as reported in [15]. It has also been verified that a single point dipole in the close vicinity of the cylinder is scattered without amplification; the latter is only found with circular arrays of dipoles of zero instantaneous dipole strength. In contrast, the point dipole would be amplified if approached to the edge of the half-plane [11].

5. Small-scale in-air experiment

5.1. Setup

For validation purposes, a small-scale experiment has been performed, aimed at confirming the asymptotic amplification associated with the compact Green's function. The experiment is made in air for simplicity. A three-bladed propeller of 63 mm blade-tip diameter is mounted at one end of a cylindrical hub of diameter 27 mm and length 170 mm, as shown in Fig. 5-a. It is powered by a Maxon DC-motor (type 2 322.980–52) of 21 mm diameter inserted in the hub at two regimes, referred to as the low speed (11800 rpm) and high speed (14800 rpm), corresponding to blade-tip Mach numbers of about 0.1 and 0.14, respectively. The scattering cylinder has a diameter of 60 mm and a length of 1 m. The propeller plane is at mid-length of the cylinder. The hub is placed parallel to the cylinder at varying distance D, by means of diametrically sliding rods of 5 mm diameter. The latter are believed to have a negligible effect on the relative variations of the sound resulting from changes in D.

The mock-up is installed vertically in an anechoic room, according to the sketch in Fig. 5-b. Twelve 1/4" microphones (GRAS type 46BE) are placed at azimuths $j\,2\pi/12$ $(0 \leq j \leq 11)$ in the plane of the propeller disk, at a measuring distance r_x of 1.2 m from the cylinder axis. The condition of acoustic far-field at the first BPF is already ensured at this distance. The origin of coordinates is taken on the cylinder axis because the asymptotic scattering involves secondary sources distributed on the cylinder, which are much more efficient than the primary sources on the blades. The microphones are inserted horizontally into L-shaped vertical supports of 8 mm diameter, pointing toward the cylinder axis. This instrumentation is believed to cause negligible spurious scattering.

The two rotational speeds correspond to BPF of 590 Hz and 740 Hz. They are tested for various values of the axis-to-axis distance D. The shortest distance of 65 mm only leaves a minimum gap of about 2 mm between the blade tip passages and the cylinder. The largest one is of 168 mm. The corresponding dimensionless parameters are summarized in Table 1.

The experiment is mainly aimed at highlighting the characteristic amplification, with the generation of the mode -1. The precise blade design and a complete inspection of the propeller aerodynamics are beyond the scope of the study. This would have typically required advanced optical flow-measurement techniques at the very small scale of the experiment, in order to avoid intrusiveness.

Table 1
20 Hz-bandwidth peak levels and Helmholtz numbers at the BPF as a function of D (mm), for both tested rotational speeds.

	$D = 65$	$D = 70$	$D = 85$	$D = 95$	$D = 168$
low speed (dB)	48.3	49.1	42.55	38.2	35.3
$(ka = 0.35)$ kD	0.71	0.76	0.92	1.04	1.83
$k(D - [R_0 + a])$	0.030	0.084	0.25	0.35	1.15
high speed (dB)	55.1	52.7	48	46	45.7
$(ka = 0.44)$ kD	0.88	0.96	1.16	1.30	2.30
$k(D - [R_0 + a])$	0.037	0.11	0.31	0.45	1.45

5.2. Sound-pressure spectra

Typical spectra (PSD, power spectral densities) of the measured sound pressure, averaged on all microphones of the array, are shown in Fig. 6. The averaging provides a relevant global characterization of the radiated sound field, as long as the angular variations along the array remain small. This is the case for the direct field at the first two BPF tones, as well as for the total field in the presence of the cylinder in the compact configuration of minimum separation D, at least for the BPF, as shown in Fig. 7. The significant angular variations for the installed configuration at twice the BPF, in Fig. 7-b, are not believed to question the final conclusions. The resolution in Fig. 6 is of 1 Hz and the acquisition time of 30 s ensures convergence. Two spectra are superimposed on each plot, one for the shortest value of D (65 mm) and the other one for $D = 85$ mm (in Fig. 6-a & c) and $D = 140$ mm (in Fig. 6-b & d). This enables to identify the amplification of the first two BPF tones, marked by the double arrows. The associated values of the tonal-noise level differences are also reported on the plots, after integration of the PSD in 20-Hz bandwidths centered on the peak values. This eliminates the possible time variations of the rotational speed. These differences are slightly larger than the peak-to-peak differences illustrated by the double arrows.

A significant increase of the third tone can also be noticed at the higher rotational speed (Fig. 6-c & d). The key result is that the levels at the first two BPF tones dramatically increase as the propeller approaches the cylinder, to the shortest distance. The increase at the BPF is of 11.1 dB for the low speed and of about 12.6 dB for the high speed, going from $D = 140$ mm to $D = 65$ mm. It is worth noting that the sound spectrum also includes other tones not directly related to aerodynamic propeller noise. The shaft rotational frequency and some of its harmonics are attributed to mechanical imbalance. They are not amplified by cylinder scattering, because they do not have the required modal structure for this. Indeed, the amplification operates only on source-modes, in other words equivalent circular distributions of plus and minus dipole sources which globally behave like sources of higher polar orders. The amplification is a specificity of the BPF tones, expressed by Eq. (1) and investigated in the next section. The multiple tonal, haystack-like signature at higher frequencies, beyond 2BPF, is probably produced by the electric motor. It is also ignored in this study.

Additional results discussed for completing the argumentation are shown in Fig. 8. Fig. 8-a compares the averaged sound spectrum measured for the minimum distance $D = 65$ mm to averaged free-field spectra measured after removing the cylinder. Two positions of the propeller axis, namely at the center of the microphone array and shifted by $D = 168$ mm, are considered, providing nearly the same BPF tone levels, highlighted by small ellipses. The figure illustrates the maximum amount of scattering by the cylinder.

The increase of propeller tonal noise associated with the presence of the cylinder could result from any of two mechanisms. The first one is the amplification inherent to the asymptotic regime of the Green's function, expected from the theoretical analysis of Section 4. The second one is the possible generation of stronger blade-loading harmonics, as an effect of higher stationary flow distortions. Indeed, the flow the propeller would have in free field, especially around the blade tips, can be modified as the blades get close to the cylinder because of some flow blockage. Investigating such aerodynamic changes would require a specific instrumentation, well beyond the scope of the present study. Therefore, simple indirect considerations only based on far-field acoustic measurements are used to state about that point. The first step is a complementary measurement performed after replacing the cylinder by a large rigid plate mounted vertically and approached at the same distance to the blade tips as in the configuration $D = 65$ mm. The plate is 1.2 m high and 0.6 m wide, the propeller being placed close to its center point. It is believed to have aerodynamic effects similar to those of the cylinder at the scale of the blade tip-flow details, which makes qualitatively the same order of magnitude of the blade-loading harmonics expected, if any. However, unlike the cylinder, the plate causes pure reflection of the direct sound from the propeller. For plate dimensions much larger than the wavelength, the image principle would hold. Applying this principle to a simple point source at vanishing distance, a doubling of the measured sound-pressure amplitude, thus a maximum sound increase of 6 dB, would be found for measuring locations facing the plate, instead of the amplification. The case of the propeller is less simple. The result of the test is reported in Fig. 8-b. But because the averaging procedure leading to Fig. 6 would make no sense in the presence of the plate, the spectra have been averaged only on the two microphones located around ±15° from the direction normal to the plate. The BPF tone levels in free-field condition and with the plate installed, with 20-Hz bandwidth integration, are 42.5 dB and 46.3 dB, respectively, whereas the level reaches 58.6 dB with the cylinder in the configuration $D = 65$ mm. The increase of $46.3 - 42.5 = 3.8$ dB remains compatible with a sound-reflection effect, and suggests that the regeneration of blade-loading harmonics is either moderate or negligible. The much higher sound increase of $58.6 - 42.5 = 16.1$ dB is logically attributable to the aforementioned amplification mechanism.

Approaching a side-plate to a rotor disk has also been found to increase the tonal noise in previous studies, because of both the reflection effect and the aerodynamic interaction. The latter is presumably more noticeable at high speeds, when an axial flow and

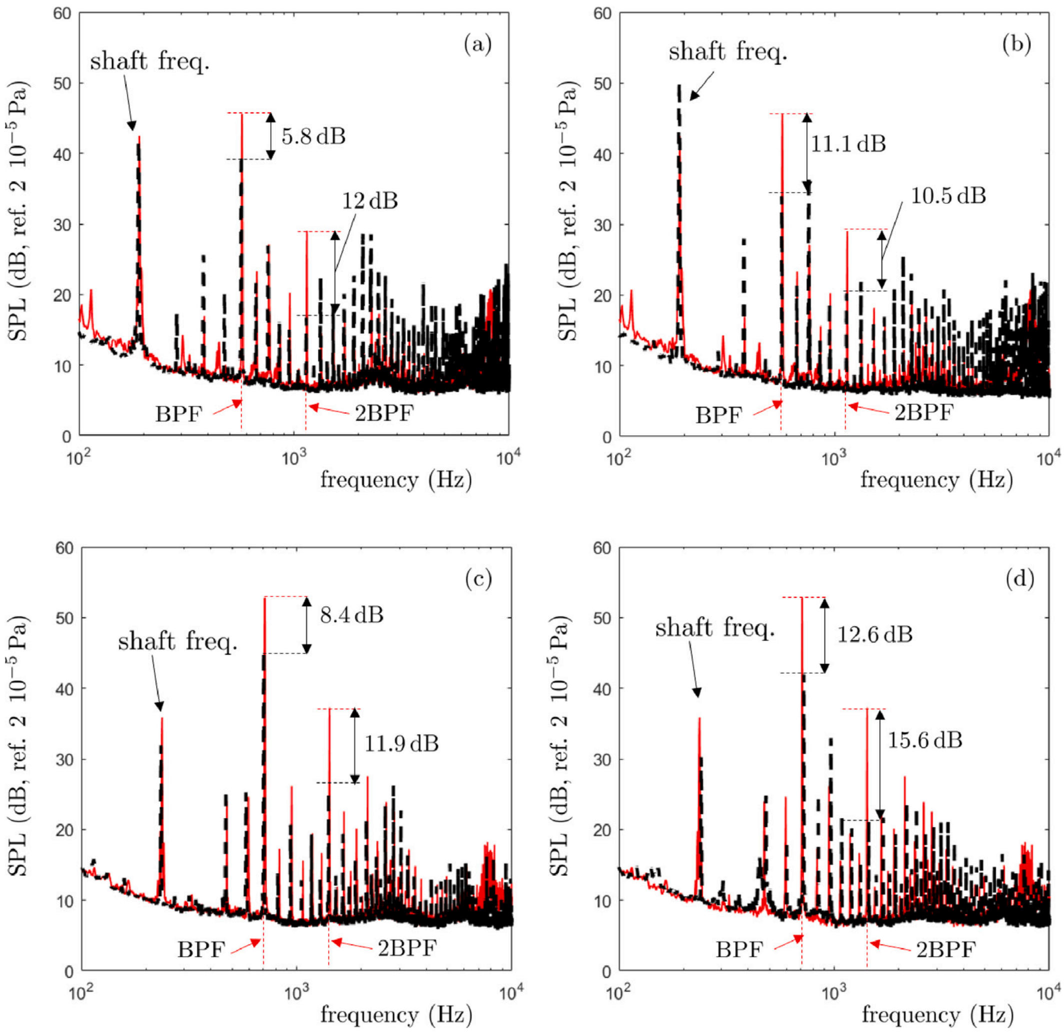

Fig. 6. Compared sound-pressure spectra for axis-to-axis distances $D = 65$ mm (red) and $D = 85$ mm (black) in the left column ((a) & (c)), and for $D = 65$ mm (red) and $D = 140$ mm (black) in the right column ((b) & (b)). (a) & (b): low rotational speed; (c) & (d): high rotational speed. (For interpretation of the references to color in this figure legend, the reader is referred to the web version of this article.)

the associated boundary layer develop over the plate. Whatmore & Lowson reported various tonal noise increases of up to 8–10 dB in such a configuration, for a typical tip Mach number around 0.22 and a blade-tip radius of 33 cm [18]. Such a strong effect is not expected in the present study because of the lower Mach numbers of 0.1 and 0.14, at the two tested speeds. Yet the 8–10 dB increase can be considered as a maximum expectable effect, which remains much lower than the actual increase observed in the presence of the cylinder.

Apart from the variations in tone levels, all spectra in Figs. 6 and 8 exhibit similar broadband noise levels below 1.7 kHz, and small differences at higher frequencies. The latter are not interpreted in the present study. Indeed, the broadband noise is much lower than the tonal noise of interest, and always limited by a threshold of about 7 dB corresponding to the electronic background noise.

The main outcome of this section is that reducing the gap between the blade tips and a reflecting plate causes tonal noise increases which remain much lower than those with the same gap and the cylinder. It is concluded that the large noise increase observed with the cylinder is rather a sound-scattering effect than an aerodynamic effect. This is confirmed in the next section by performing an expansion of the sound field in the rotor-disk plane into azimuthal modes of radiation.

5.3. Modal content of the radiated field

Free-field formulations of tonal propeller noise, reminded in Section 2.1, indicate that the sound field of any harmonic of the BPF is a sum of spinning modes of radiation, as viewed from the propeller reference frame $(\mathbf{e}_X, \mathbf{e}_Y, \mathbf{e}_Z)$ (Fig. 1). The scattering of this direct field by the cylinder generates a secondary field also made of modes, as viewed from the cylinder reference frame.

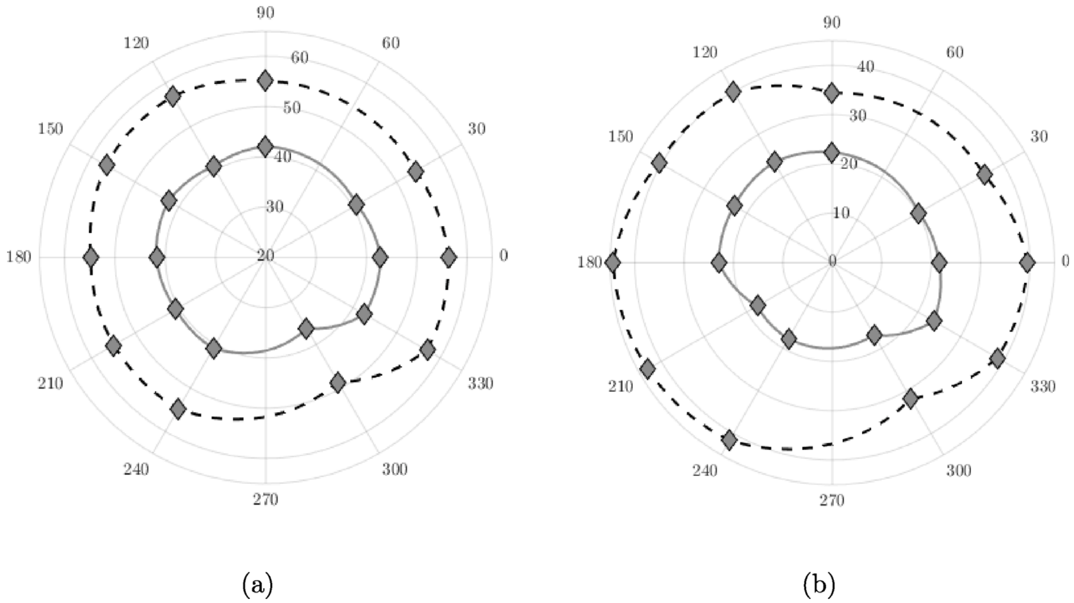

Fig. 7. Directivity diagrams in the (x, y) plane at the BPF (a) and twice the BPF (b), with linear interpolation between measuring positions (symbols ⋄). (—): Free-field measurements for the centered propeller ($D = 0$). (- - -): installed propeller at $D = 65$ mm. Different dB scales in the two sub-plots.

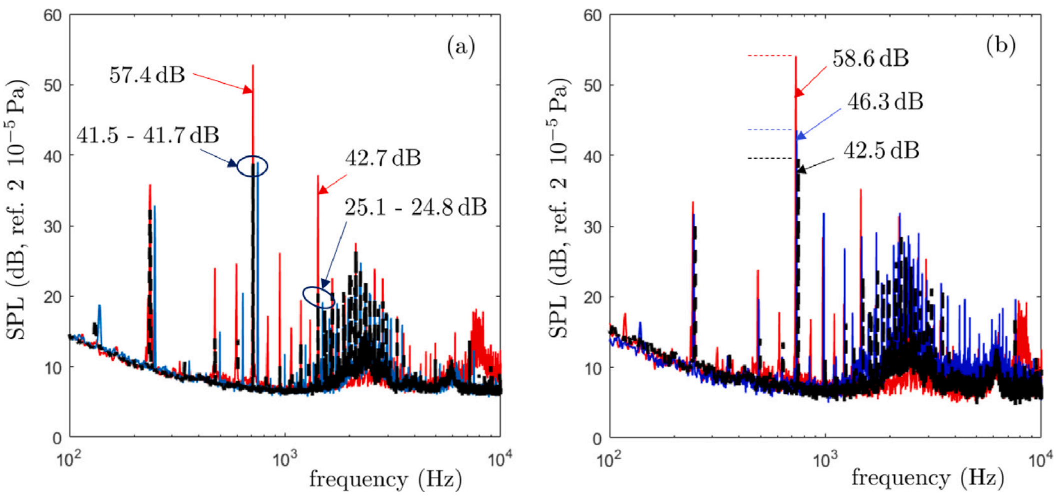

Fig. 8. (a): free-field sound spectra of the propeller, at the center of the microphone array (blue) and shifted by $D = 168$ mm (black), compared to the spectrum measured with the cylinder installed at $D = 65$ mm (red); average over the complete array. (b): sound-pressure spectra of the propeller, in free field (black), close to a reflecting plate (red, blade-tip to wall gap 2 mm) and close to the cylinder (blue, $D = 65$ mm); two-microphone average. High speed case, BPF = 740 Hz. (For interpretation of the references to color in this figure legend, the reader is referred to the web version of this article.)

In the installed configuration, the propeller axis is displaced by an amount D off the origin of the center of the microphone array. This makes the modal signature of the direct sound radiated by the propeller hard to recognize in the modal expansion of the total sound field. Indeed, the latter is performed taking the cylinder axis as origin, whereas the former makes sense with origin on the propeller axis. Except for vanishing ratio D/λ, a direct propeller mode of order n is interpreted by the array processing as a range of modes, in the reference frame of the cylinder. This effect is assessed in the present section for an easier interpretation of results.

The free-field sound pressure at any point of the array circle of radius r_x centered on the cylinder axis, thus in absence of the latter, and for the mode n of amplitude A_n, is expressed as an integral over the source circle, as

$$p_{ar}(r_x, \theta_x) = \frac{\mathrm{i}\,k}{4} A_n \int_0^{2\pi} \mathrm{e}^{\mathrm{i}\,n\phi} \frac{\mathrm{H}_1^{(1)}(k r_\phi)}{r_\phi} \left[R_0 \cos\zeta - R\cos(\phi + \zeta - \xi)\right] \mathrm{d}\phi\,, \tag{21}$$

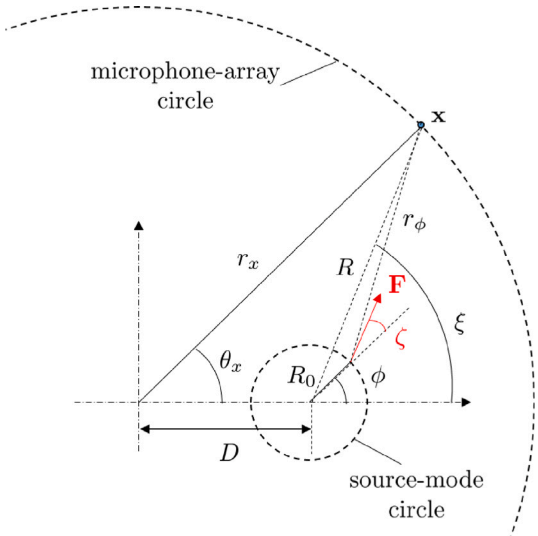

Fig. 9. Coordinates of a point on the circle of the microphone array and relative to the off-axis source circle.

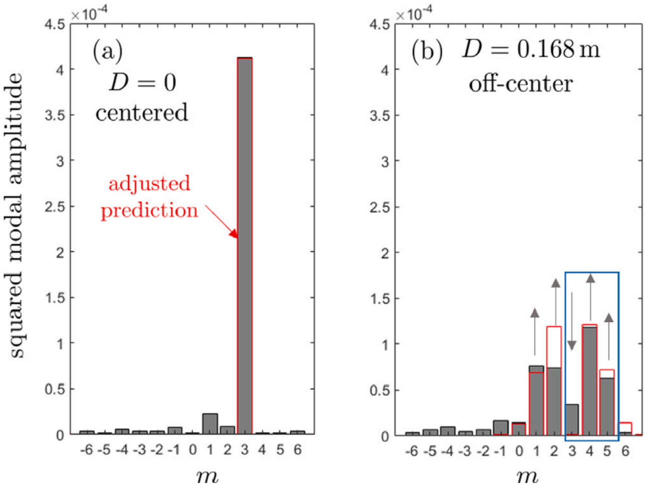

Fig. 10. Measured modal structure of the free-field sound of the propeller at the BPF. High-speed case. (a): propeller at the center of the microphone array; (b): off-centered propeller. Measured values as gray bars and indicative prediction as empty red bars. (For interpretation of the references to color in this figure legend, the reader is referred to the web version of this article.)

with

$$r_\phi = \sqrt{R_0^2 + R^2 - 2\,R R_0\,\cos(\xi - \phi)}\,,$$

if (ξ, R) denote the polar coordinates of the observer with respect to the center of the source circle (see Fig. 9). The transposition in the cylinder reference frame is ensured by the relations

$$R = \sqrt{r_x^2 + D^2 - 2\,D r_x\,\cos\theta_x}\,, \qquad \tan\xi = \frac{r_x\,\sin\theta_x}{r_x\,\cos\theta_x - D}.$$

For the considered mode n, the post-processing leads to the complex-valued modal amplitudes

$$p_m = \frac{1}{2\pi}\int_0^{2\pi} p_{ar}(r_x,\theta_x)\,\mathrm{e}^{-\mathrm{i}\,m\,\theta_x}\,\mathrm{d}\theta_x\,. \tag{22}$$

The free-field noise of the model propeller has been also measured in the experiment, after removing the cylinder, for two positions of the propeller axis: one at the center of the array, and the other one at the location corresponding to the maximum separation $D = 0.168$ of the installed configuration (see spectra in Fig. 8). For this test, the propeller-and-hub element shown in Fig. 5-a has been mounted alone, at the tip of a vertical bar, in order to avoid azimuthal flow distortions. The modal spectra, as

Table 2
Expected BLH orders s and associated Bessel-function weighting factors and spinning-mode orders n at the BPF. Effective values of the factor and expected significant s orders bold-faced.

s	-1	**0**	**1**	**2**	3	4	5	6
$B\,J_{B-s}(BM)$	neg.	$4.6\,10^{-3}$	**0.065**	**0.62**	**2.87**	**−0.62**	**−0.065**	$-4.6\,10^{-3}$
n	4	3	2	1	0	−1	−2	−3

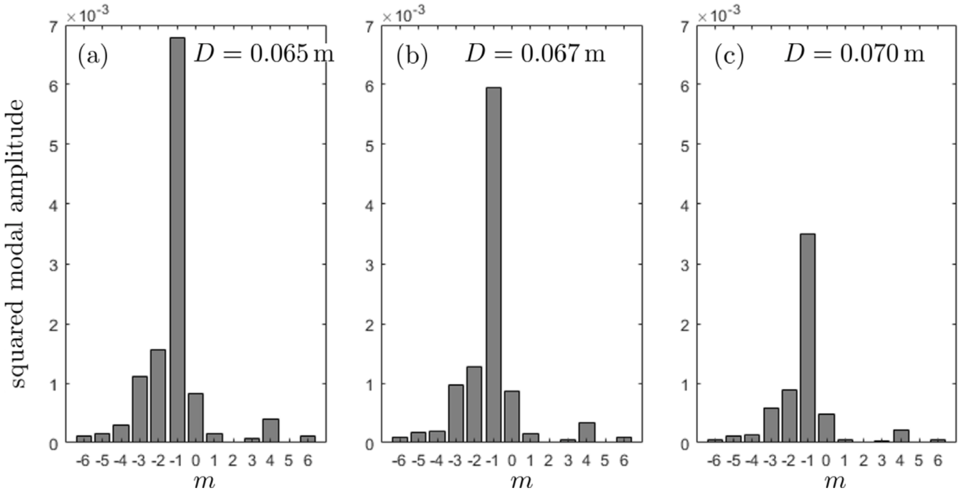

Fig. 11. Measured modal structure of the total field of the installed propeller at the BPF. High-speed case, short distances D.

produced by the microphone-array processing, are plotted as gray bars in Fig. 10. Subplots (a) and (b) refer to a propeller center-point coinciding with the center of the array and displaced by $D = 0.168$ m from that center, respectively. In the first case, the mode $m = n = B = 3$ dominates the radiated field, with only a negligible contribution of other modes. This rotor-locked mode is the signature of the combined steady-loading noise and thickness noise. The result confirms that residual distortions are negligible, as expected for an axisymmetric configuration. As the propeller is moved away from the array center, the same processing generates a range of modes, amongst which the modes of orders (1,2,4,5), corresponding to 3 ± 1 and, less prominently, 3 ± 2, dominate, whereas the mode 3 is strongly reduced. Bar-graph predictions of this modal-scattering effect produced by Eqs. (21) and (22) with an arbitrary amplitude are also plotted for indicative comparison. They confirm the redistribution of the mode orders. In view of the overall qualitative agreement, the procedure can be used to identify the free-field signature of the propeller in the modal expansions performed in the presence of the scattering cylinder. Similar results, not shown, have been observed at the lower rotational speed. More generally, the trend has been verified that, for the largest values of D, the propeller mode n is mainly seen as the modes $m = n - 1$ and $m = n + 1$.

The radiation efficiency of steady-loading noise is a matter of blade number and tangential Mach number M. In the propeller-disk plane and in the far field, at the μ^{th} harmonic of the BPF, it is determined from the value $\mu B\,J_{\mu B}(\mu B\,M)$ where B is the blade number. This value is about $4.6\ 10^{-3}$ in the present case at the BPF ($\mu = 1$) and about $4.46\ 10^{-5}$ at twice the BPF ($\mu = 2$). Despite its low but not vanishing value, the factor explains why the mode $n = B = 3$ can be detected in the free-field modal expansion at the BPF.

Results of the modal analysis for the installed configuration including the propeller and the cylinder, at the higher rotational speed, are reported in Figs. 11–13, for the smallest, intermediate and largest axis-to-axis distances D, respectively. In each figure, the same scale is used for the three plots. For small values of D (Figs. 11-a to c), a strong emergence of the mode $m = -1$ is observed, the amplitude decreasing with increasing distance. This still holds for intermediate distances, as seen for instance in Fig. 12-a. Modes of orders between −3 and 0 are also found, though with much lower amplitudes. These negative orders are out of the range of expected BLH, as shortly discussed below at the light of the values in Table 2. They are attributed to cylinder scattering.

In fact, the modal analysis of the total field for varying axis-to-axis distance D is limited by the lack of information about actual values of the BLH. The origin of the latter lies in any distortion of the mean flow through the propeller disk (deviation from pure axisymmetry). Their amplitudes *a priori* vary with D because the distortion is a matter of aerodynamic blockage by the cylinder. The propeller also ingests a residual wake from the sliding rods shown in Fig. 5; this contributes to the BLH. Furthermore, the amount of scattering differs for different source-mode radii. Now the radial (spanwise) distribution of the forces is unknown, which prevents from producing a quantitative analysis. Yet qualitative arguments are enough to confirm the amplification mechanism investigated in this work. Firstly, the distortions due to the vicinity of the cylinder are expected to generate low-order BLH, say typically corresponding to s between −2 and +2 (bold-faced values in Table 2). Secondly, as shown by Eq. (1), the weighting factor $B\,J_{B-s}(BM)$ involved at the BPF is significant only for small values of $|B - s|$, which leads to only retain the range of values also reported bold-faced in the second line of Table 2. Only the overlapping bold-faced ranges in the table are likely to produce a significant contribution. This suggests that, irrespective of their unknown amplitudes, the BLH of orders $s = 1, 2$ dominate in the

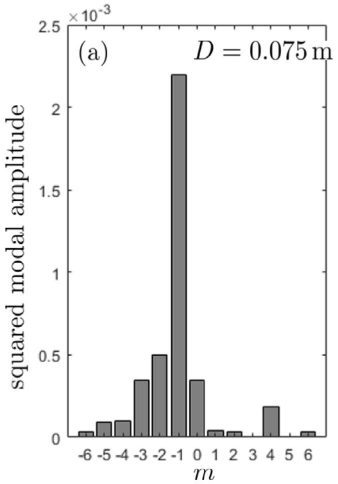

Fig. 12. Measured modal structure of the total field of the installed propeller at the BPF. High-speed case, intermediate distances D.

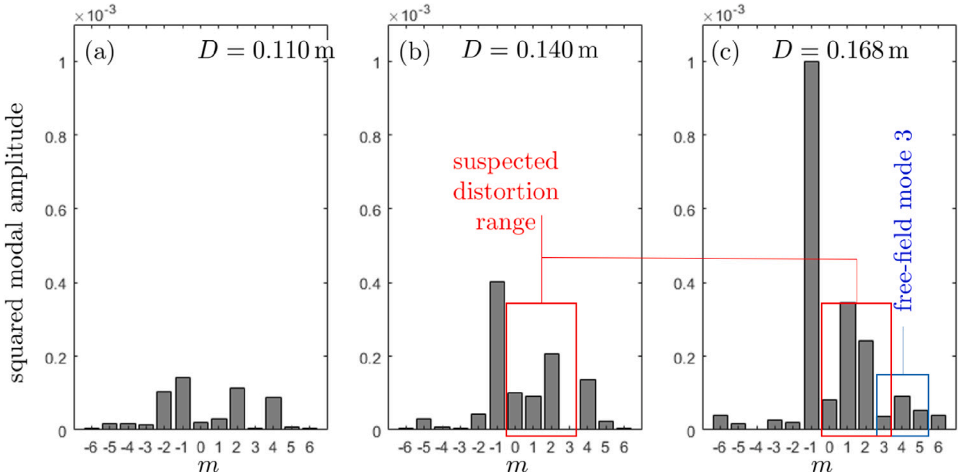

Fig. 13. Measured modal structure of the total field of the installed propeller at the BPF. High-speed case, large distances D.

direct field of the installed propeller, in addition to the steady-loading noise. The main effect of the off-origin positioning is to generate the modes $m = 0$ and 2 for $s = 1$ and the modes $m = 1$ and 3 for $s = 2$ in the modal expansion computed from the microphone array.

The results for the largest axis-to-axis distances, Fig. 13, seem contradictory. Indeed, the mode amplitudes increase significantly with increasing distance D, with a dominant mode -1. The observed modes of orders 0,1,2, with moderate amplitudes, are those expected from an azimuthal distortion. They are highlighted by the red boxes in Figs. 13-b and c. It is worth noting that the modes 3,4,5 grouped in the blue box in Fig. 13-c have the same amplitudes as in the free-field configuration reported in Fig. 10. This suggests that the rotor-locked mode $n = 3$ in the reference frame of the propeller is still recognizable in the modal expansion. But it is of secondary importance in the total sound field. It is conjectured that the 'free-field' modes 1 and 2 in Fig. 10-b are overwhelmed by the same modes as generated by the additional distortion in the presence of the cylinder and sliding bars, in Fig. 13-c. Such a distortion could only be detected by advanced and non-intrusive optical techniques, well beyond the scope of the present study.

5.4. Tonal-noise amplification

The amplification rate of the BPF harmonics by the asymptotic behavior of the Green's function is finally addressed in this section. The observed variations of the tonal noise with the separation D are also compared with theoretical predictions.

Fig. 14 displays the BPF tone level, integrated in a 20-Hz bandwidth, as a function of the separation D, for the low and high rotational speeds. A log-scale is used for D. Despite unexplained irregularities in the low-speed case for small separations (diamond symbols, (⋄)), the same overall trend is found. The BPF tone levels decrease at the same rate for both speeds, for small and

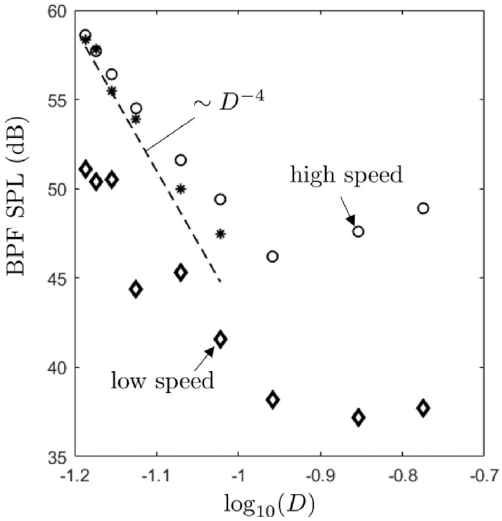

Fig. 14. BPF tone level as a function of separation D, with 20-Hz bandwidth integration, for the high-speed (∘) and low-speed (⋄) cases. D^{-4}-law featured by the dashed line. (∗): relative levels of the mode $m = -1$ from Figs. 11 and 12, shifted for comparison.

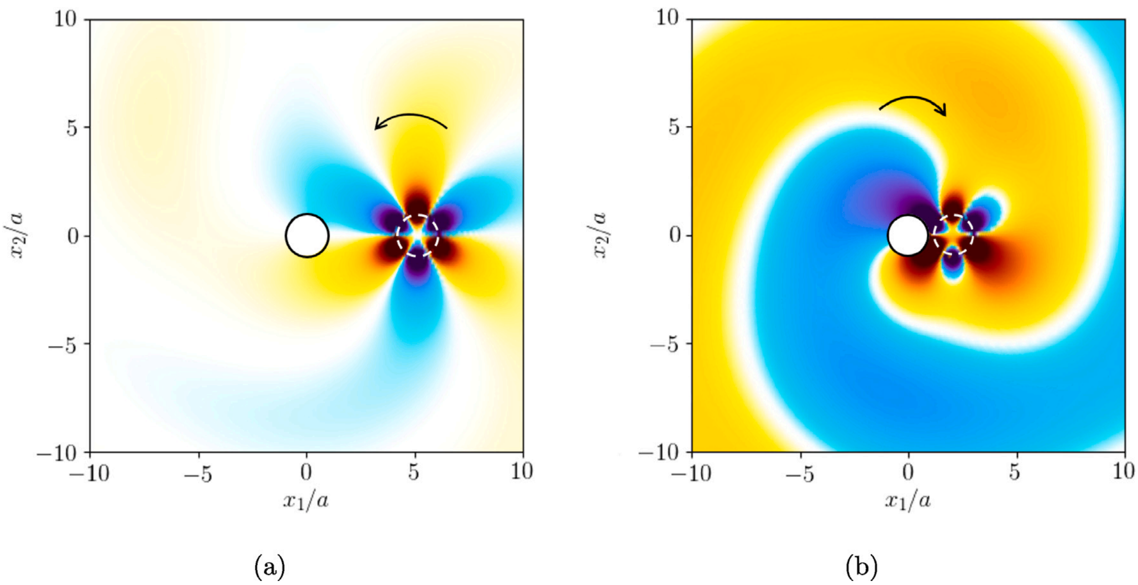

Fig. 15. Predicted instantaneous pressure maps of a circular array of phased dipoles in the presence of a scattering cylinder, for the counterclockwise rotor-locked mode $n = 3$. Cases of weak scattering, D = 168 mm (a) and compact regime, D = 65 mm (b), featuring the formation of the mode $m = -1$. Parameters representative of the experiment. Source mode featured as dashed circle, same arbitrary color scale on both plots. The arrows indicate the directions of rotation of the direct mode $n = 3$ in subplot (a) and of the scattered mode $m = -1$ in subplot (b).

moderate separations D. The global difference of about 6 dB between low-speed and high-speed data is expected from the scaling law of dipole sources with the sixth power of flow speed in aeroacoustics [3]. Indeed, using the rotational speed as reference, $60 \log_{10}(14800/11800) = 5.9$. Then the sound slightly increases for larger separations. The amplitudes of the mode $m = -1$ in relative decibels, as deduced from Figs. 11 and 12, are also plotted as star symbols (∗), for the high-speed case. The values are shifted vertically to fit the measured tone levels (symbols ∘) at the shortest separations. Both negative slopes are close to each other, confirming that the tone level and its decrease are mostly determined by the mode $m = -1$.

If it is assumed that blade-loading harmonics are only generated at a negligible level as the propeller is moved very close to the cylinder, the modal structure of the direct sound field of the propeller is dominated by the mode $n = 3$. The amplitude of the associated scattered field is determined by the cylinder mode $m = -1$, according to Eq. (13). A sound-pressure amplitude proportional to D^{-4} is expected. This asymptotic law is reported as the dashed line in Fig. 14. The actual rate of decrease is slightly slower, suggesting that modes of orders $n \neq 3$ are also generated.

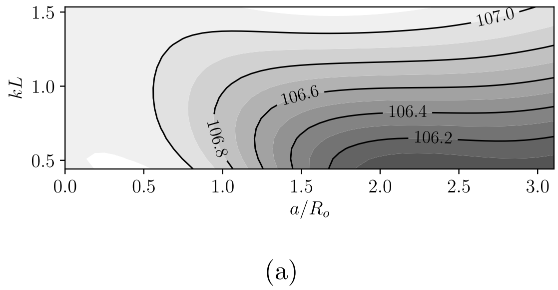

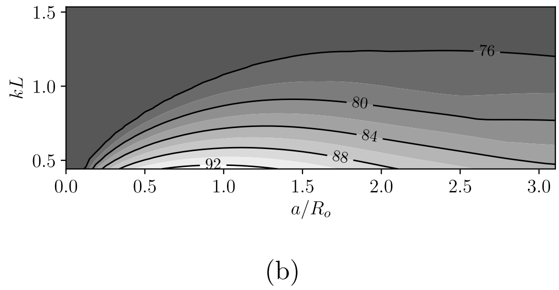

Fig. 16. Total-field SPL maps of individual source-modes in arbitrary decibel scale, as a function of the distance L between cylinder edge and source-mode center and of the ratio a/R_0. $kR_0 = 0.44$; modes $n = 1$ (a) and $n = 3$ (b). Parameters representative of the experiment.

The main outcomes of the experiment are twofold. Firstly, the tonal noise at the BPF combines the rotor-locked mode $n = 3$ and a couple of adjacent modes. Secondly, these modes are dominantly scattered as the mode $n = -1$ as the propeller-cylinder distance decreases, with a strong amplification. This is expected from the present theoretical developments. Finally, typical instantaneous pressure maps computed with the exact analytical formulation are shown in Fig. 15, in order to illustrate the features of the combined direct and scattered fields. These test cases reproduce configurations of the experiment, with the rotor-locked source-mode $n = 3$ as primary sound. The characteristic attenuation distance, over which the direct field of this mode decreases down to very low values, has the same order of magnitude as the mode radius, as suggested by the size of the six spots on the maps, one per half lobe. The separation of $D = 168$ mm, Fig. 15-a, largely exceeds the attenuation distance of the mode. Therefore, the scattered field from the cylinder is relatively weak, because of the same amplitude as the local direct field at the location of the cylinder surface. In contrast, the small separation of $D = 65$ mm, Fig. 15-b, is substantially smaller than the attenuation distance. In this case, the scattered field is of the same order of magnitude as the direct field close to its source. But because the generated mode $m = -1$ is now radiating instead of evanescent, the scattered field is much larger than the direct field at large distances. This example illustrates the amplification mechanism.

The three parameters involved in the diffraction mechanism are the distance L between the cylinder surface and the source-mode center, and the two radii a and R_0. The analytical model based on the exact Green's function, Eq. (5) allows to investigate extended ranges of these parameters, in order to identify critical areas of amplification. Such a parametric study, covering configurations representative of the experiment, is illustrated for the source-modes $n = 1$ and $n = 3$ in Figs. 16-a and 16-b, respectively, with SPL maps. On each map, an arbitrary decibel scale is used, so that only the variations make sense. Indeed, the source strengths are unknown and the information of interest is the effect of the cylinder on the radiating properties of a mode. Because the mode $n = 1$ already radiates efficiently in free field, cylinder scattering only induces moderate modifications on it. As a result, the map in Fig. 16-a exhibits variations of about 1 dB.

In contrast, the mode $n = 3$ is evanescent in free field and experiences strong amplification by asymptotic cylinder scattering. The map in Fig. 16-b now exhibits large variations. The SPL increases as the source-mode to cylinder distance L is reduced. Two other important conclusions can be drawn. Firstly, the SPL drops for $a \ll R_0$, which means that the amplification no longer operates for vanishing cylinder size. Secondly, a maximum amplification regime is found for $a/R_0 \simeq 1$. These important features could be the basis for the definition of guidelines when designing a global architecture.

6. Application to hub scattering

The scattering effect of the hub or the center body of a propeller on the emitted tonal noise has been pointed out in air by various authors [19–22]. The question also arises for the hub of marine propellers, in connection with the possible amplification effect inherent to the compact regime. It is answered in this section, with a straightforward application of the exact analytical model of Sections 3 and 4, in the special case of coaxial cylinder and source-mode, as depicted in Fig. 17. The generic configuration of Fig. 1 is simply reconsidered by setting $D = 0$, so that the source-mode component of propeller tonal noise is centered at the origin of the cylinder coordinates (r_x, θ_x), with the condition $R_0 > a$. The same compactness conditions $kR_0 \ll 1$ and $ka \ll 1$ are again assumed. The same exact analytical computations and source-mode discretization procedure are applied.

The effect of center-body scattering on the amplitude of the radiated field is assessed by averaging the far-field sound pressure for all observation angles, and by comparing it to the free-field radiation. The result is reported for various mode orders in Fig. 18, where the Sound Pressure Level difference ΔSPL is plotted as a function of the ratio a/R_0, for a fixed value of ka. The radiated sound is found to increase as the sources get closer to the cylinder surface, for the same assumed dipole strength. For any mode order, the sound increase reaches +6 dB as the source-mode radius approaches the hub radius, $a/R_0 \sim 1$. This result is intuitively expected by similarity with the image principle, according to which sources approaching a rigid plane have their radiated sound pressure doubled. It is also recovered by an asymptotic analysis of the Green's function, considering $D = 0$ with the following set of conditions:

$$kr_x \gg 1,\ ka \ll 1,\ kR_0 \ll 1,\ \frac{a}{R_0} \sim 1\,.$$

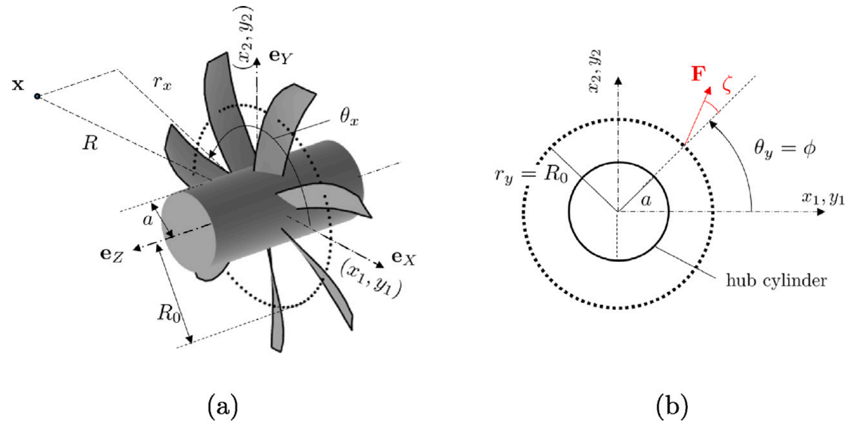

Fig. 17. Coordinates and main notations for coaxial source-mode and scattering cylinder. (a): three-dimensional propeller-and-hub configuration, (b): two-dimensional reduction, featuring the source-mode as dotted-line circle. Note that $D = 0$ with respect to Fig. 2.

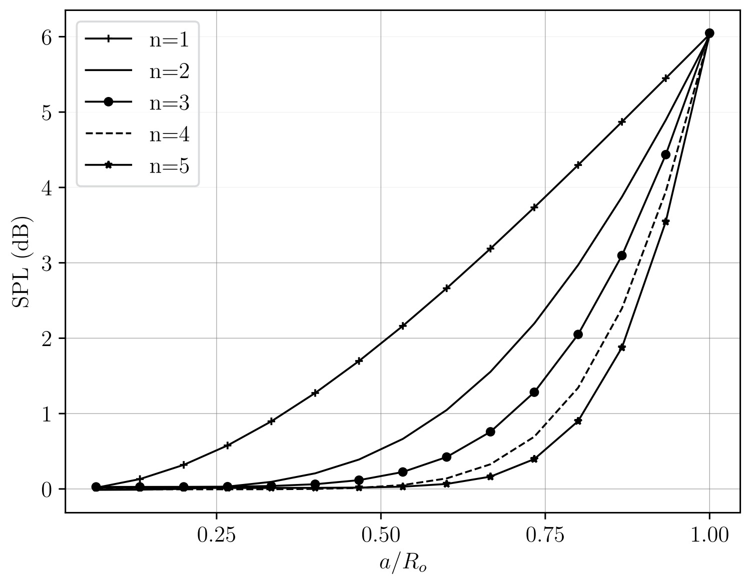

Fig. 18. Averaged far-field Sound Pressure Level radiated by various source-mode orders n in the presence of a hub, as a function of a/R_0. $ka = 0.10$.

Following the same procedure as in Section 4, the asymptotic derivations, not further detailed, are made substantially simpler because the sources are centered, leading to $r_y = R_0$ and $\theta_y = \phi$. The point dipole of angular coordinate ϕ along the source circle is the same for radial and tangential forces, and it is expressed as $F_s^R, F_s^T \propto e^{in\phi}$. Finally, the leading order of the total field is obtained as

$$p_{1as}(r_x, \theta_x) = 2\, p_{0as}(r_x, \theta_x), \tag{23}$$

which is consistent with the exact analytical model. This maximum amount of sound-pressure increase remains well below the amplification evidenced in previous sections for off-axis source-modes. In that sense, hub scattering is free of true amplification, which can be interpreted as follows. The amplification by compact Green's function behavior is typical of higher-order source-modes. Because the latter are compact distributions of dipoles with zero instantaneous balance, they have at most a quadrupole-like efficiency in free field, by virtue of partial cancellation. Any off-centered scattering body in compact vicinity of a source-mode generates very different elementary scattered fields for the constitutive point dipoles. This imbalance makes the resulting partial cancellation much less pronounced, thus the radiation much more effective: in fact, the mode radiates with the basic dipole-like efficiency. The situation is different for an axisymmetric center body because the amount of scattering is the same for all constitutive elements of a source-mode, leading to zero imbalance. As a result, the at-most quadrupole-like behavior is preserved, and the total-reflection increase of 6 dB is the maximum expected effect.

7. Three-dimensional considerations

A three-dimensional complement of the analysis is given in this section for completeness, to confirm the sufficiency of the two-dimensional approach. For this, an infinite cylinder is considered, and an axial force component is compared to a tangential component of same strength. The three-dimensional Green's function for the infinite rigid cylinder can be obtained from the two-dimensional one by Fourier transform with respect to the axial coordinate. Indeed the obtained mathematical problem for the transformed axial wavenumber component k_3 is the two-dimensional one for the modified wavenumber $\gamma = \sqrt{k^2 - k_3^2}$. The sought solution is obtained by applying the inverse Fourier transform on the two-dimensional solution for k_3. Similar developments have been reported by Kingan & Self [20] with an additional mean-flow effect, for application to aeronautical propellers. Accounting for the fact that the imaginary part of the factor $\mathrm{e}^{\mathrm{i}\, k_3 (x_3 - y_3)}$ gives a zero contribution to the inverse transform, the Green's function reads

$$\begin{aligned} \mathrm{G}(\mathbf{x}, \mathbf{y}) = {} & \frac{\mathrm{i}}{4\pi} \int_0^{\infty} \sum_{m=0}^{\infty} a_m \cos[m(\theta_x - \theta_y)] \cos[k_3 (x_3 - y_3)] \\ & \times \left[\mathrm{H}_m^{(1)}(\gamma\, r_x) \left(\mathrm{J}_m(\gamma\, r_y) - \beta_m(\gamma\, a)\, \mathrm{H}_m^{(1)}(\gamma\, r_y) \right) \right] \mathrm{d}k_3, \end{aligned} \tag{24}$$

with

$$\gamma = \sqrt{k^2 - k_3^2}, \qquad \beta_m(\gamma\, a) = \frac{\mathrm{J}_{m-1}(\gamma\, a) - \mathrm{J}_{m+1}(\gamma\, a)}{\mathrm{H}_{m-1}^{(1)}(\gamma\, a) - \mathrm{H}_{m+1}^{(1)}(\gamma\, a)}.$$

In the implementation, the integral is discretized and truncated as a finite sum. The tests reported in this section considered 40 dipole sources for the discretization of a source-mode, and an upper limit of the integral of 3.5 k with a discretization step of 0.0027 k, ensuring convergence of the results. Figs. 19 and 20, plotted for the axial and tangential force components of the mode $n = 1$, respectively, show instantaneous sound-pressure maps on an observation sphere of radius 1 m, with an arbitrary color scale, and an illustration of three-dimensional directivity diagrams. The parameters are representative of the experiment. In both cases, the free-field radiation is compared to the radiation in presence of the scattering cylinder. With the same assumed source strength, the maximum sound pressure amplitude with the tangential force was found 5 times higher than with the axial force, with a different directivity. This force radiates no sound in the plane of the source-mode. Furthermore, as already pointed out with the two-dimensional model, no amplification is found, the mode $n = 1$ being already efficient in free field. Computations, not detailed here for conciseness, were repeated in the same conditions with the mode $n = 3$. The same strong amplification for the tangential force component has been observed as in the two-dimensional calculations, as expected. The radiation from the axial force was also found amplified by the same amount, with more significant sound regeneration on axis, because of the imbalance introduced in nearly-cancelling sources. However, the maximum of free-field sound pressure amplitude was now about 20 times higher for the tangential force, corresponding to a difference of 26 dB inherent to the different orientation of the forces. For both components, the amplification involves the formation of the contrarotating mode -1. The main conclusion is that for largely amplified modes, thus modes of higher order n in the compact regime, the axial force component has a much weaker intrinsic efficiency. For the mode $n = 1$, the difference of efficiency between both components, though again in favor of the tangential one, is reduced; but this mode is not amplified. Finally, the amplification of propeller tonal noise caused by the lateral vicinity of a body is a general feature, much more pronounced for the force components in the rotation plane. Radiating features predicted by the three-dimensional model only confirm the key findings of previous sections, based on the two-dimensional formulation, with structuration of the mode -1. The two-dimensional predictions also compared very well with the trends measured in the experiment. This justifies *a posteriori* that the detailed analysis is developed in a two-dimensional context. The three-dimensional extension, including the axial force component, would become essential for applications to a real propeller, provided that a propeller design is made available, and to arbitrary observation angles. The blade surface would be discretized, the scattering problem solved for each blade element of the discretization, and the total sound field reconstructed by linear superposition. The basic features highlighted with the present model would be directly transposable, obviously giving more importance to sources distributed at the blade tips, because they would be more amplified by virtue of their shorter distance to the scattering cylinder. The extension itself is beyond the scope of the present work, rather focused on the basic amplification mechanism. The extension also implies considering a cylinder of finite length, for physical consistency, in which case the aforementioned Green's function is no longer valid. Such a configuration, and *a fortiori* that of a realistic hull geometry, would require a numerical solving of the Helmholtz equation. This has not been considered in the present study, dedicated to what a pure mathematical approach can produce. Some remarks can be made about this choice. Firstly, the inspection of the scattering by an infinite cylinder, and by extention also by a finite-length, elongated body, has its major interest in directions normal to the cylinder axis, because the equivalent sources of the scattered field are dipoles normal to the surface. This is a first argument for a two-dimensional reduction, keeping in mind that the three-dimensional approach is not essential to understand the amplification by compact scattering. Secondly, comparing the infinite-cylinder model calculations with numerical simulations by a boundary-element method, for validation purpose, would imply truncation of the meshed surface of the cylinder. This would make the comparison questionable. It can be conjectured that a finite-length body would also cause amplification by compact scattering of a source-mode, provided that the latter is placed close enough to the body end, and off-centered. Indeed, imbalance would similarly be induced between the elementary sources of the source-mode.

Another aspect is that the axial force component on the blades may be a dominant source of noise for marine propellers, if related to vibrations, as pointed out, for instance, by Zhou et al. [?]. This is a complementary topic, not addressed here. Yet the amplification mechanism addressed in the present work could partly operate on vibration noise. The condition for this is that a structural mode of vibration of the whole propeller has the same structure of spinning mode, with circular distributions of phased dipoles of zero instantaneous balance. Investigating this could be the matter for future work.

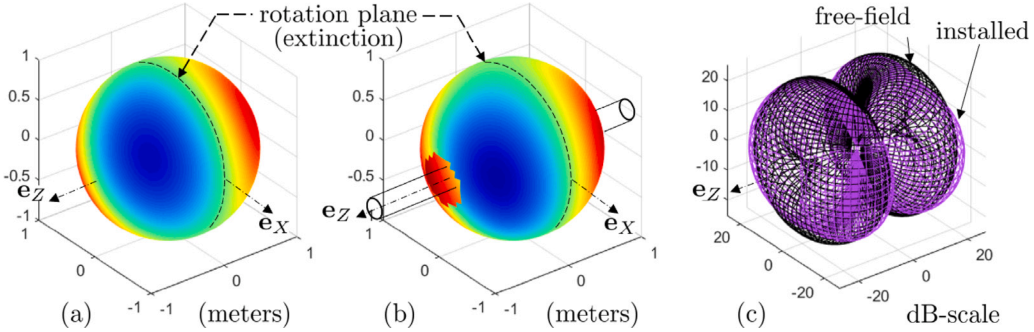

Fig. 19. Radiation properties of the spinning mode $n = 1$ for an axial force component. (a,b): instantaneous sound-pressure patterns on a far-field observation sphere, for the free-field and installed configurations, respectively. (c): compared directivity diagrams. $f = 700$ Hz, $a = 30$ mm, $R_0 = 30$ mm, $D = 65$ mm. Cylinder shown, not-to-scale, on subplot (b).

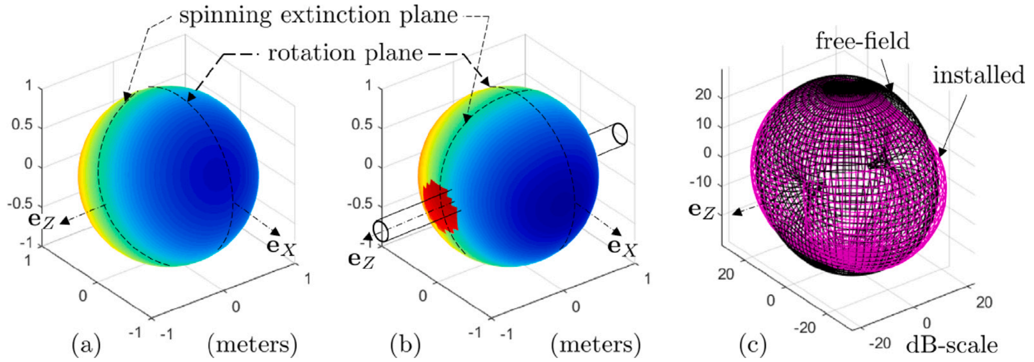

Fig. 20. Radiation properties of the spinning mode $n = 1$ for a tangential force component. (a,b): instantaneous sound-pressure patterns on a far-field observation sphere, for the free-field and installed configurations, respectively. (c): compared directivity diagrams. $f = 700$ Hz, $a = 30$ mm, $R_0 = 30$ mm, $D = 65$ mm. Cylinder shown, not-to-scale, on subplot (b).

8. Conclusion

A simple, two-dimensional analytical formulation has been implemented to highlight fundamental aspects, that are expected to dominate the tonal noise radiated by a marine propeller installed close to a scattering hull. For mathematical tractability, a rigid cylinder has been selected as generic hull geometry. The formulation is based on the Green's function of the cylinder for the Helmholtz equation, on the one hand, and on the notion of source-modes, on the other hand. The source-modes are circular distributions of phased sources, reproducing the free-field, or direct, radiation modes of rotor tonal noise. They are defined in the reference frame of the propeller by their integer orders, equal to their numbers of angular periods. In a real configuration, the direct modes are a consequence of the operation of the propeller in the mean-flow distortion around the hull. The scattered field can also be described in term of modes, defined in the reference frame of the cylinder. In view of the extremely low Mach numbers in marine applications, the mean relative axial fluid motion is neglected, in both the free-field and installed radiation models. The effect of the flow distortion is concentrated in the definition of the sources and the associated direct modes. Furthermore, because of the very low Helmholtz numbers based on the size of a domain encompassing the source-modes and the scattering cylinder cross-section, an asymptotic regime of diffraction is encountered. This is why an asymptotic formulation has been compared to the exact calculations to interpret the results. The analytical approach provides a detailed insight into the physics of sound scattering, mode by mode. Quite generally, direct modes of higher orders (larger than 1) are found to only generate evanescent waves in free field, whereas they experience a very strong amplification in close vicinity of the cylinder. This amplification results from the interaction of the near field of the sources with the cylinder. The most spectacular result is that it generates the scattered radiating mode or order 1, whatever the direct mode order is, with inversion of the phase rotation. In contrast, the direct mode of order 1 is already very efficient in free field, because of its compactness, and only experiences a moderate amount of diffraction. The symmetric mode of order 0 radiates negligible sound, both in free-field and in the presence of the cylinder, according to the two-dimensional model. These compact-scattering properties of the cylinder differ from what obstacles of other geometry would produce on similar source-modes, for instance in a case of propeller blade tips operating close to wing edges.

A small-scale experiment has also been carried out in air, only based on acoustic measurements, with Helmholtz numbers representative of marine applications. For this, a three-bladed model propeller and a rigid cylinder of characteristic diameters of about 60 mm were selected, the blade passing frequency being around 750 Hz. The tests were performed in an anechoic chamber with variable relative positions, resorting to a circular array of far-field microphones to get access to the direct and scattered angular modes. The experiment clearly confirmed the amplification mechanism and the emergence of the contra-rotating mode of order 1, which validates the mathematical developments. Tests with the three-dimensional cylinder Green's function confirmed the key results of the two-dimensional approach. The sound from the axial component of the blade forces is also amplified by the same mechanism, but it has a much weaker free-field efficiency, compared to other components.

The main outcomes suggest that the short distance of marine propellers to the hull of a ship could result in a dramatic acoustic installation effect, that cannot be neglected and should be taken into account at the early stage of a global design approach. The features and amplitude of the scattered field are found very sensitive to all involved parameters, such as direct mode orders, relative propeller-cylinder distance and so on. Up to that point, the simple tools proposed in this work are well suited to investigate primary effects in a very fast way. The theoretical study will be extended to more realistic configurations in a future work, by resorting to a numerical determination of the Green's function tailored to arbitrary hull geometry.

CRediT authorship contribution statement

Elina Cros: Conceptualization, Methodology, Software, Validation, Formal analysis, Investigation, Writing – original draft, Writing – review & editing, Visualization. **Michel Roger:** Conceptualization, Methodology, Validation, Formal analysis, Investigation, Resources, Writing – original draft, Writing – review & editing, Supervision, Project administration. **Gilles Serre:** Conceptualization, Validation, Investigation, Resources, Writing – review & editing, Supervision, Project.

Declaration of competing interest

The authors declare that they have no known competing financial interests or personal relationships that could have appeared to influence the work reported in this paper.

Data availability

No data was used for the research described in the article.

Acknowledgments

This work was supported by Naval Group and the LABEX CeLyA, France (ANR-10-LABX-0060) of *Université de Lyon*, within the program *Investissements d'Avenir* (ANR-11-IDEX-0007) operated by the French National Research Agency (ANR).

Appendix. Derivation of integrals

The analytical formulation of the asymptotic regime leads to integrals that can be obtained in closed-form expressions, making use of tables by Gradshteyn & Ryszik [23] and noting that the odd-function parts can be discarded from the integrands. They are listed in this appendix. For $n > 1$, the individual integrals involved in the scattered-field formulation are found as:

$$\int_{-\pi}^{\pi} \frac{\cos\phi\, \mathrm{e}^{\mathrm{i}\,n\,\phi}}{r_y^4}\,\mathrm{d}\phi = \frac{\pi}{D^4}\,\frac{(-R_0/D)^{n-1}}{[1-(R_0/D)^2]^3}\left\{4\left(\frac{R_0}{D}\right)^2 + n\left[1-\left(\frac{R_0}{D}\right)^4\right]\right\}, \tag{A.1}$$

$$\int_{-\pi}^{\pi} \frac{\sin\phi\, \mathrm{e}^{\mathrm{i}\,n\,\phi}}{r_y^4}\,\mathrm{d}\phi = \frac{n\,\mathrm{i}\,\pi}{D^4}\,\frac{(-R_0/D)^{n-1}}{[1-(R_0/D)^2]}, \tag{A.2}$$

$$\int_{-\pi}^{\pi} \frac{\mathrm{e}^{\mathrm{i}\,n\,\phi}}{r_y^4}\,\mathrm{d}\phi = \frac{2\pi}{D^4}\,\frac{(-R_0/D)^{n}}{[1-(R_0/D)^2]^3}\left[n+1-(n-1)\left(\frac{R_0}{D}\right)^2\right]. \tag{A.3}$$

and those involved in the free field formulation as:

$$\int_{-\pi}^{\pi} \frac{\cos\phi\, \mathrm{e}^{\mathrm{i}\,n\,\phi}}{r_y^2}\,\mathrm{d}\phi = \frac{\pi\,(-R_0/D)^{n-1}}{D^2\,[1-(R_0/D)^2]}\,[1+(R_0/D)^2], \tag{A.4}$$

$$\int_{-\pi}^{\pi} \frac{\cos 2\phi\, \mathrm{e}^{\mathrm{i}\,n\,\phi}}{r_y^2}\,\mathrm{d}\phi = \frac{\pi\,(-R_0/D)^{n-2}}{D^2\,[1-(R_0/D)^2]}\,[1+(R_0/D)^4], \tag{A.5}$$

$$\int_{-\pi}^{\pi} \frac{\sin\phi\, \mathrm{e}^{\mathrm{i}\,n\,\phi}}{r_y^2}\,\mathrm{d}\phi = \frac{\mathrm{i}\,\pi}{D^2}\,(-R_0/D)^{n-1}, \tag{A.6}$$

$$\int_{-\pi}^{\pi} \frac{\sin\phi\,\cos\phi\, \mathrm{e}^{\mathrm{i}\,n\,\phi}}{r_y^2}\,\mathrm{d}\phi = \frac{\mathrm{i}\,\pi}{2D^2}\,(-R_0/D)^{n-2}\,[1+(R_0/D)^2], \tag{A.7}$$

$$\int_{-\pi}^{\pi} \frac{\mathrm{e}^{\mathrm{i}\,n\,\phi}}{r_y^2}\,\mathrm{d}\phi = \frac{2\,\pi}{D^2}\,\frac{(-R_0/D)^{n}}{[1-(R_0/D)^2]}. \tag{A.8}$$

Special developments are required for the mode $n = 1$. The corresponding integrals read, for the scattered-field formulation:

$$\int_{-\pi}^{\pi} \frac{\sin\phi\, \mathrm{e}^{\mathrm{i}\,\phi}}{r_y^4}\, \mathrm{d}\phi = \frac{\mathrm{i}\,\pi}{D^4\,[1-(R_0/D)^2]}\,, \tag{A.9}$$

$$\int_{-\pi}^{\pi} \frac{\cos\phi\, \mathrm{e}^{\mathrm{i}\,\phi}}{r_y^4}\, \mathrm{d}\phi = \frac{\pi}{D^4\,[1-(R_0/D)^2]^3} \left[1 + 4\left(\frac{R_0}{D}\right)^2 - \left(\frac{R_0}{D}\right)^4\right], \tag{A.10}$$

$$\int_{-\pi}^{\pi} \frac{\mathrm{e}^{\mathrm{i}\,\phi}}{r_y^4}\, \mathrm{d}\phi = \frac{4\pi}{D^4}\, \frac{(-R_0/D)}{[1-(R_0/D)^2]^3} \tag{A.11}$$

and for the free-field formulation:

$$\int_{-\pi}^{\pi} \frac{\cos\phi\, \mathrm{e}^{\mathrm{i}\,\phi}}{r_y^2}\, \mathrm{d}\phi = \pi\, \frac{1+(R_0/D)^2}{D^2[1-(R_0/D)^2]}\,, \tag{A.12}$$

$$\int_{-\pi}^{\pi} \frac{\cos 2\phi\, \mathrm{e}^{\mathrm{i}\,\phi}}{r_y^2}\, \mathrm{d}\phi = \pi\, \frac{1+(R_0/D)^2}{D^2[1-(R_0/D)^2]}(-R_0/D)\,, \tag{A.13}$$

$$\int_{-\pi}^{\pi} \frac{\sin\phi\, \mathrm{e}^{\mathrm{i}\,\phi}}{r_y^2}\, \mathrm{d}\phi = \frac{\mathrm{i}\,\pi}{D^2}\,, \tag{A.14}$$

$$\int_{-\pi}^{\pi} \frac{\sin\phi\, \cos\phi\, \mathrm{e}^{\mathrm{i}\,\phi}}{r_y^2}\, \mathrm{d}\phi = \frac{\mathrm{i}\pi}{2D^2}(-R_0/D)\,, \tag{A.15}$$

$$\int_{-\pi}^{\pi} \frac{\mathrm{e}^{\mathrm{i}\,\phi}}{r_y^2}\, \mathrm{d}\phi = 2\pi\, \frac{(-R_0/D)}{D^2[1-(R_0/D)^2]}\,. \tag{A.16}$$

References

[1] J.F. Williams, D. Hawkings, Sound generation by turbulence and surfaces in arbitrary motion, Philos. Trans. R. Soc. Lond. A (264) (1969).
[2] J. FfowcsWilliams, D. Hawkings, Theory relating to the noise of rotating machinery, J. Sound Vib. 10 (1) (1969) 10–21.
[3] M. Goldstein, Aeroacoustics, McGraw-Hill Book Company, New York, 1976.
[4] F. Farassat, The derivation of a thickness noise formula for the far-field by isom, J. Sound Vib. 64 (1979) 159–160.
[5] Y. Wei, Y. Shen, S. Jin, P. Hub, R. Lan, S. Zhuang, D. Liu, Scattering effect of submarine hull on propeller non-cavitation noise, J. Sound Vib. 370 (2016) 319–335.
[6] C. Testa, L. Greco, Prediction of submarine scattered noise by the acoustic analogy, J. Sound Vib. 426 (2018) 186–218.
[7] M. Roger, K. Kucukcoskun, Near-and-far field modeling of advanced tail-rotor noise using source-mode expansions, J. Sound Vib. 453 (2019) 323–354.
[8] A. Carazo, M. Roger, M. Omais, Analytical prediction of wake-interaction noise in counter-rotating open rotors, in: 17th AIAA/CEAS, Aeroacoustics Conference, 2011.
[9] M.S. Howe, Sound generation in a fluid with rigid boundaries, in: Acoustics of Fluid–Structures Interactions, Cambridge, 1998, pp. 164–166.
[10] J.E. Ffowcs Williams, L.H. Hall, Aerodynamic sound generation by turbulent flow in the vicinity of a scattering half-plane, in: Journal of Fluids Mechanics, 1970.
[11] M. Roger, S. Moreau, K. Kucukcoskun, On sound scattering by rigid edges and wedges in a flow, with applications to high-lift device aeroacoustics, J. Sound Vib. 362 (2016) 253–275.
[12] M. Goldstein, Unified approach to aerodynamic sound generation in the presence of solid boundaries, J. Acoust. Soc. Am. (1974) 497–509.
[13] D.B. Hanson, D.J. Parzych, Theory for noise of propellers in angular in- flow with parametric studies and experimental verificatio, 1993, Final Report United Technologies Corp., Windsor Locks, CT. Standard Div., Vol. 1.
[14] M. Abramowitz, I. Stegun, Handbook of Mathematical Functions, DOVER, New-York, US, 1970.
[15] M. Roger, Near-field fan noise modelling and installation effects due to scattering surfaces, in: Fan Noise 2007, 2007.
[16] P.M. Morse, K.U. Ingard, Theoretical Acoustics, Princeton University Press, Princeton, New Jersey, 1986.
[17] X. Gloerfelt, F. Pérot, C. Bailly, D. Juvé, Flow-induced cylinder noise formulated as a diffraction problem for low mach numbers, J. Sound Vib. 287 (2005) 129–151.
[18] M. Whatmore, Some effects of ground and side planes on the acoustic output of a rotor, 1973.
[19] A. Parry, D. Crighton, Asymptotic theory of propeller noise—Part I: Subsonic single-rotation propeller, AIAA J. 29 (1991) 2031–2037.
[20] M. Kingan, R. Self, Open rotor tone scattering, J. Sound Vib. 331 (2012) 1806–1828.
[21] S. Glegg, Effect of centerbody scattering on propeller noise, AIAA J. 29 (1991) 572–576.
[22] M. Kingan, P.S. Institute, Open rotor centrebody scattering, J. Sound Vib. 333 (2014) 418–433.
[23] I.S. Gradshteyn, I.M. Ryzik, Tables of Integrals, Series and Products, Academic Press, New-York, US, 1980.